Materials & Design 225 (2023) 111550

Contents lists available at ScienceDirect

Materials & Design

journal homepage: www.elsevier.com/locate/matdes

Size effect on bending strength of glued laminated timber predicted by a numerical simulation concept including discrete cracking

Christoffer Vida *, Markus Lukacevic, Georg Hochreiner, Josef Füssl

Institute for Mechanics of Materials and Structures, TU Wien, Karlsplatz 13/202, 1040 Vienna, Austria

HIGHLIGHTS

- Simulation campaign that covers 8840 glued laminated timber configurations.
- Size effect is quantitatively predicted for beams up to 3300 mm depth.
- The influence of the length to depth ratio is compared to Weibull's strength theory.

GRAPHICAL ABSTRACT

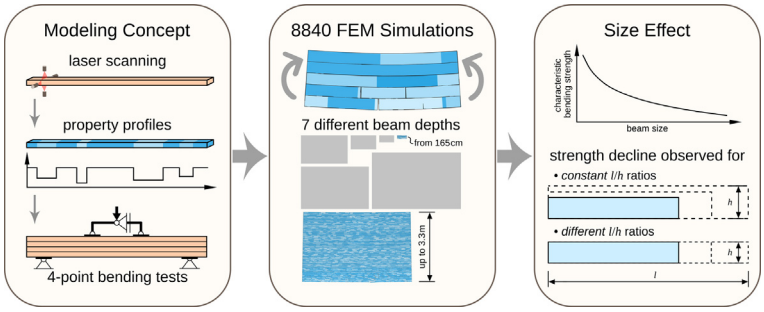

ARTICLE INFO

Article history:
Received 11 August 2022
Revised 7 December 2022
Accepted 25 December 2022
Available online 30 December 2022

Keywords:
Size effect
Glued laminated timber
XFEM
Failure mechanisms

ABSTRACT

The dimensions, particularly the depths, of glued laminated timber (GLT) beams are continuously increasing to realize, e.g., wide-span hall constructions or flexible office buildings. However, experimental investigations of large beams are unavailable because of the tremendous effort involved. Numerical simulation campaigns represent an alternative, but their results are heavily influenced by the modeling strategy, and therefore, a different influence of the beam depths on the bending strength was obtained. To predict this influence, also called size effect, we carried out a simulation program covering 8840 GLT beams ranging from 165 mm to 3300 mm in depth, using advanced modeling concepts including discrete cracking and plasticity.

We observed a decreasing characteristic bending strength with increasing beam depths and an almost constant mean modulus of elasticity for both considered strength classes. Additionally, the influence of the beam length on the bending strength is analyzed, and it is shown that this influence can be described reasonably well with a simple analytical model based on Weibull's strength theory. In conclusion, the effective material behavior of GLT is affected by its dimensions. For large beams, this influence is difficult to obtain experimentally; however, numerical simulation campaigns seem to be a promising way to accomplish this.

1. Introduction

Wood is a naturally growing resource, which is used as a raw material for various building products, e.g., glued laminated timber (GLT). Manufacturing GLT beams from individual wooden boards resolves size restrictions and improves mechanical properties through homogenization. GLT consists of lamellas, built by finger jointed wooden boards, glued together on top of each other. The wooden boards, in general, are characterized by a high degree of variability, induced by the natural growth process, causing the material properties to have a much more pronounced fluctuation than that of materials like steel or brick. Consequently, potential

* Corresponding author.
E-mail address: christoffer.vida@tuwien.ac.at (C. Vida).

https://doi.org/10.1016/j.matdes.2022.111550
0264-1275/

weak points, such as knots and knot groups, can be found in random distribution within GLT beam layouts. Therefore, a sound understanding of effective material properties, which depend on the beam size, is required. Herein, we focus on the influence of the beam size on the longitudinal modulus of elasticity (MOE) and the bending strength in four-point bending tests.

The material properties of GLT beams together with their determination are provided in DIN EN 14080 [1]. There, the characteristic longitudinal MOE $E_{0,g,05}$ is defined as 5/6 of the mean longitudinal MOE $E_{0,g,mean}$ without any adjustment for the beam depth. On the other hand, the characteristic bending strength $f_{m,g,k}$ is valid explicitly for the reference beam depth: $h_{ref} = 600$ mm. The experimental determination of the properties is carried out through four-point bending tests according to DIN EN 408 [2] (Fig. 1). All length measurements in the test setup are coupled to the beam depth h. The length ℓ (beam region under constant bending moment) is always six times the depth h, according to the dimensional reference ratio: $\ell/h = 6.0$. Herein, a characteristic value corresponds to the 5% quantile.

According to DIN EN 1995-1-1 [3], an increase of the characteristic bending strength $f_{m,g,k}$ is allowed for GLT beams with depths smaller than the reference depth h_{ref}. For those cases, $f_{m,g,k}$ may be adapted by the factor k_h:

$$k_h = \min \begin{cases} \left(\frac{600}{h}\right)^{0.1} \\ 1.1 \end{cases} \quad \text{for} \quad h \leqslant 600\,\text{mm}. \tag{1}$$

The k_h factor in Eq. (1) is based on Weibull's strength theory [4], referring to strength as a statistical property and expressing the probability of brittle failure based on weak points within a stressed volume. This influence of the size on wood properties [5–8] is often referred to as size effect and also known from other building materials, e.g. concrete [9–12]. Nevertheless, the concept behind Eq. (1) is not applied for larger beam depths than the reference depth, nor is it able to explicitly consider different beam lengths to depths ratios.

Comprehensive experimental studies [13–15] on beams up to the reference depth were performed in the 1990s. More recently, experimental studies with smaller sample sizes [16,17] focused on material property distributions within the layout and their influence on the entire beam. Fink et al. [18] recently examined GLT beams with a depth of up to 1000 mm. However, in the literature most of the testing was performed on GLT beams with a depth of about 300 mm.

Numerical simulations represent an efficient alternative or extension to complex experiments. The development of modeling approaches to simulate GLT beams started already in the 1980s, e.g., with the well-known *Karlsruher Calculation Model* [19–22]. An updated version of the approach was used to realize multiple studies regarding the size effect [23–28]. Aside from this approach, a further probabilistic modeling approach for GLT beams [29–32] was developed. More recently, the extended finite element method (XFEM) was employed in an approach to estimate the bending strength of GLT beams made from hardwoods [33–35].

With ongoing improvements of these approaches, the numerical investigation of the size effect on the bending strength for large GLT beams became feasible. Hence, Fink et al. [32] and Frese and Blaß [24] conducted numerical studies including beam depths of 1200 mm and up to 3000 mm, respectively. Their results showed contradictory trends regarding the influence of the beam size on the characteristic bending strength . Further, only beam sizes following the dimensional reference ratio according to DIN EN 408 [2] were analyzed. So there is a significant knowledge gap here, leading to uncertainties and discussions among engineers in the design of large GLT beams, which are used more and more frequently.

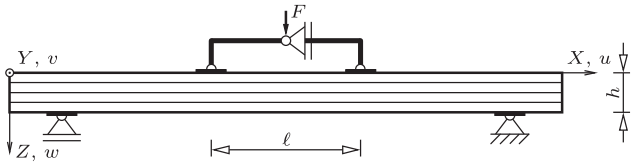

Fig. 1. Four-point bending test setup for a GLT beam with the depth h, loaded by a constant bending moment over the length ℓ.

To fill this knowledge gap and to assess the size effect of GLT beams, we apply a numerical approach to model GLT beam sections subjected to a constant bending moment. The used material properties for the wooden boards are derived from a sample of actual wooden boards, which were virtually reconstructed and analyzed [36]. With the distribution of knots and knot groups from the actual boards, the approach features Weibull's strength theory [4] automatically. The so-called lamination effect [37] is considered by the layout composed of the virtualized boards. The lamination effect accounts for the reinforcing of weak points by neighboring lamellas, which homogenizes the GLT material properties. Local failure mechanisms are considered by implementing two discrete crack directions, vertical cracks within the boards and horizontal cracks between the lamellas. Vertical cracks are realized within the framework of XFEM. This implementation allows for quasi-brittle material behavior, which mainly affects beams of smaller size [5]. The formation of horizontal cracks enables continuous crack patterns between vertical cracks in adjacent lamellas with a horizontal offset . The horizontal cracks are employed by using cohesive surface failure. Additionally, the influence of plastic effects in the compression zone of the beams is examined.

This paper provides a broad view on the size effect of GLT beams. It presents material property distributions for different beam sizes based on simulation. The main contribution is the qualitative as well as quantitative identification of the size effect of GLT beams in terms of the effective MOE and bending strength.

The paper is structured as follows. Section 2 describes how the material properties for the wooden boards were derived and presents the applied modeling approach for GLT beam sections made from such boards. The proposed approach is verified and experimentally validated in Section 3. The obtained distributions for the effective MOE E_{GLT} and bending strength f_b are given in Section 4, which subsequently provide the basis for determining the size effect of GLT beams with variable beam depths and independent lengths. The paper closes with conclusions and discusses further research focus and enhancements (Section 5).

2. Materials and methods

To simulate GLT beam sections under constant bending moment, material properties of the wooden boards are needed. Section 2.1 provides an overview of the used virtual boards replicated from real wooden boards and how their material properties were derived. Subsequently, the applied numerical modeling approach is presented in Section 2.2.

2.1. Wooden board properties

We used virtual three-dimensional boards with section-wise constant orthotropic stiffness and longitudinal tensile strength properties derived from actual wooden boards, following a concept previously applied in [17,36,38]. The distribution of the properties along the boards were provided by material property profiles (Fig. 2). The morphological characteristics of the actual board

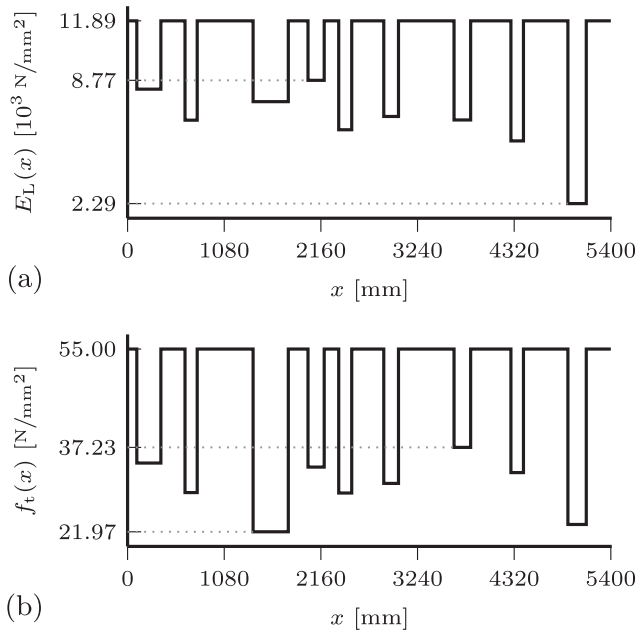

Fig. 2. Exemplary material property profiles for the section-wise constant properties of an entire virtual board with (a) the effective longitudinal MOE E_L that defines the orthotropic stiffness in conjunction with the stiffness tensor $\mathbb{C}$ and (b) the effective tensile strength f_t in longitudinal direction.

determined the individual lengths of the consecutive sections. Each section referred either to a clear wood section (CWS) for defect-free material or a weak section (WS) for a section including a single large knot or clustered knots. The boards were 5400 mm long with a planed width b of 90 mm and depth d of 33 mm. Based on the original strength grading, the boards were assigned to either strength class T14 (LS15) or T22 (LS22). Each strength class contained 140 analyzed boards. Vida et al. [38] presents an overview the virtual reconstruction of the boards and all their determined profiles.

The material properties of each board were defined by the stiffness tensor $\mathbb{C}$ and two property profiles over the entire board's length (Fig. 2). The stiffness was provided by $\mathbb{C}$ in conjunction with the profile of the effective longitudinal MOE E_L. The other profile referred to the effective tensile strength f_t in the longitudinal direction. The determination of the profiles is described in [38]. A brief overview is given in the following:

- The three-dimensional orthotropic stiffness tensor $\mathbb{C}$ was determined for each board individually, based on the micromechanical model proposed by Hofstetter et al. [39]. The density and moisture content of a board served as the primary input to the model. For CWSs, E_L in the profile was directly extracted from $\mathbb{C}$. Within WSs, E_L was determined as below. Finally, the tensor $\mathbb{C}$ was modified within each section by E_L according to the profile.
- The geometric reconstruction algorithm proposed by Kandler et al. [40] was used for the three-dimensional board reconstruction. The data for the algorithm was supplied by the information gathered during the strength grading process. The representation of knots was realized with rotationally symmetric cones.
- The effective longitudinal stiffness E_L was derived for individual WSs in a separate finite element approach outlined in [17,36,38]. For each WS, the knots and the three-dimensional fiber course were modeled according to [41,42]. To determine E_L, each WS was loaded in a displacement-controlled manner.
- The effective tensile strength f_t of WSs depended on the specific knot area ratio, as proposed by Lukacevic et al. [43]. To all CWSs, a constant strength of 55 N/mm^2 was assigned according to the findings presented in [38].

2.2. Modeling approach

For modeling GLT beam sections loaded under a constant bending moment (Fig. 3), we applied a three-dimensional finite element approach based on a previously presented approach [38]. The simulations were performed by using the finite element software Abaqus [44]. Finally, the effective MOE E_{GLT} and bending strength f_b of the modeled GLT beam section were determined. The approach considers local failure by allowing two discrete crack directions, as schematically illustrated in Fig. 3.

The length ℓ to depth h ratio of the GLT beam section (Fig. 3) was kept constant for the majority of the simulations to investigate the influence of the beam depth h. In this domain of the beam section, vertical and horizontal cracking as well as plastic deformations were allowed to take place. The vertical crack domain generally covered half of all assembled lamellas within the beam section on the side under tension. Only the beam with five lamellas had a greater vertical crack domain covering three lamellas (Fig. 3). For beams consisting of up to 20 lamellas ($h = 660$ mm), plastic deformations were allowed in all remaining lamellas on the compression side. Additionally, the constant length e of 100 mm was added on both ends to avoid disturbing the area of interest by load application effects.

Each beam section was assembled from the wooden boards presented in Section 2.1. The layout of all beam sections was homogeneous, meaning that only boards of one strength class were randomly arranged. Each placed lamella was selected by a uniformly distributed pseudo-random process consisting of the following steps:

1. Random picking of a full-length board from the entire pool of virtual boards.
2. Random longitudinal displacement of the board within the GLT beam section to define the start and end positions of the lamella.
3. Random choice of the lamella's orientation in the GLT beam layout.

Ordinary GLT beams also include finger joints to overcome restrictions on the length of individual boards. However, experimental studies [14,15] found that finger joints reach the same strengths as natural weak points. Therefore, we assume that the random allocation of lamellas with all their weak points is a reasonable representation of random GLT beam sections.

The bending moment M was applied through reference points R_i on both ends of the beam section (Fig. 3). Each reference point was placed in the center of the cross-section area and had six degrees of freedom, three displacements, u, v, and w, as well as three rotations, φ_X, φ_Y, and φ_Z. The motion of each reference point was coupled to the corresponding cross-section, which stayed planar over the entire loading course. The bending moment was imposed by a rotation ϕ around the Y axis at both reference points. At reference point R_1, the boundary conditions read as:

$$u = w = 0, \quad \varphi_X = \varphi_Z = 0, \quad \varphi_Y = -\phi. \tag{2}$$

At R_2 they read as:

$$\varphi_X = \varphi_Z = 0, \quad \varphi_Y = \phi. \tag{3}$$

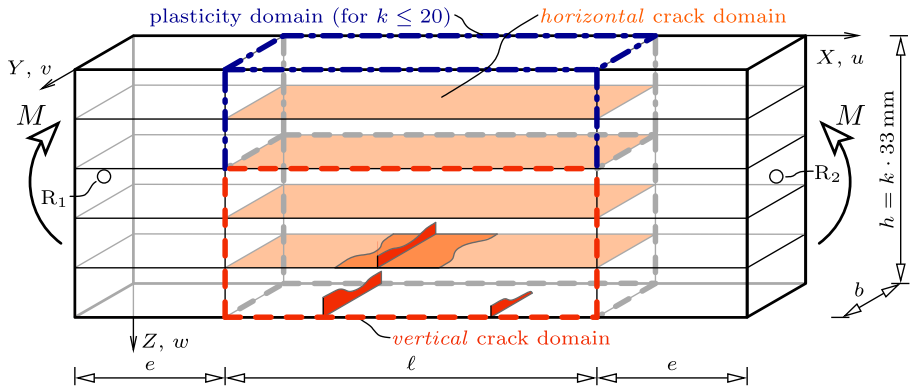

Fig. 3. Representative GLT beam section of length ℓ as used for the numerical simulations with k lamellas resulting in the depth h. The constant bending moment M and the bearing was applied at the reference points R_1 and R_2, according to Eqs. (2) and (3).

Symmetry characteristics in the middle of the width were exploited by holding the model in the *Y* direction. Thus, the model size was reduced by half.

Two failure modes were implemented for either *vertical* or *horizontal* discrete cracks (Fig. 3). Together, both modes were able to cover the effect of cracks interacting over multiple lamellas. For example, the horizontal cracking allows two vertical cracks with a horizontal offset in adjacent lamellas to become one continuous crack. The implementation is described in detail in [38], and briefly explained in the following:

- *Vertical* cracks were realized within the framework of XFEM. The method allows multiple cracks in so-called enriched regions during the loading. At the bottom half of the beam, each lamella had its own enriched region (Fig. 3). A vertical crack was initiated in an entire finite element when the average tensile stress in longitudinal direction (evaluated in the center of the finite element) exceeded the prescribed tensile strength f_t. After the initiation, the crack evolution was defined by a linear traction–separation (t–δ) law, describing the interaction between the two crack surfaces (Fig. 4a). With increasing separation, the traction decreased governed by the fracture energy $G_{f,v}$.
- *Horizontal* cracks were implemented between lamellas using the framework of cohesive surfaces. All adjacent lamellas of the beam could experience horizontal cracking (Fig. 3). A linear traction–separation law defined the traction decrease with increasing separation (Fig. 4b). The surfaces had a prescribed stiffness tensor coefficient K_{ii} and tensile/shear strength f_i, oriented normal to the surface and in the surface plane with the subscripts n, p, and q, respectively. The fracture energy $G_{f,h}$ governed the evolution of the horizontal crack.

Both failure modes used a viscous regularization scheme for stabilization control with the viscosity coefficient η. The assigned strength values and parameters are summarized in Table 1.

The general material behavior was prescribed as linear elastic. An experimental study on GLT beams [17] found that plastic deformations might occur in the zone of compressive stresses. These deformations are assumed to be relevant for small beams and high strength classes. Therefore, we implemented ideal plasticity with a multisurface failure criterion [45–47] in the upper beam half for simulations of small beams with a maximum of 20 lamellas corresponding to a depth of 660 mm (Fig. 3). The influence of considering plasticity is presented and discussed in Section 4.2. For the discretization of the model, eight-node hexahedron elements in conjunction with tri-linear shape functions were used. Section 3.1 presents a study on the mesh size and discusses the selected element size.

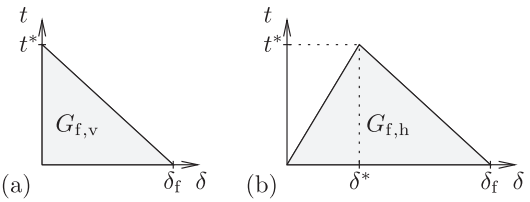

Fig. 4. Traction–separation (t–δ) law with the area representing the fracture energy G_f for (a) *vertical* cracks and (b) *horizontal* cracks, where t^* and δ^* are the traction and separation at damage initiation, respectively, and δ_f is the separation at fully evolved damage. Adapted from [44].

Table 1
Stiffness tensor coefficient K_{ii}, tensile/shear strength f_i, fracture energy G_f, and viscosity coefficient η.

vertical cracks		
$f_{t,s}$ [a]	[N/mm²]	10.0–55.0
$G_{f,v}$	[Nmm/mm²]	30.0
η_v	[–]	1×10^{-6}
horizontal cracks		
$K_{nn} = K_{pp} = K_{qq}$	[N/mm³]	1×10^{4}
f_n	[N/mm²]	5.0
$f_p = f_q$	[N/mm²]	6.0
$G_{f,h}$	[Nmm/mm²]	0.6
η_h	[–]	1×10^{-5}

[a] Tensile strength of lamella section *s*.

Global failure of the beam section was defined by the first 3% drop of the bending moment M in relation to the maximum observed bending moment M_{max}, which defined the reached load-bearing capacity. Additionally, an energy criterion was checked for every simulation to ensure a negligible influence of the applied stabilization. The criterion uses the energy terms from Abaqus [44] to relate the dissipated energies, i.e., E_{ALLVD} referring to the vertical cracks and E_{ALLCD} to the horizontal cracks, to the total strain energy E_{ALLIE} without E_{ALLCD}:

$$f = \frac{E_{ALLVD} + E_{ALLCD}}{E_{ALLIE} - E_{ALLCD}} \leqslant 5\%. \tag{4}$$

Finally, the effective MOE E_{GLT} and bending strength f_b were determined according to beam theory. The evaluation of E_{GLT} used the relation between the applied rotation ϕ and the corresponding bending moment M at two specified loading points. DIN EN 408 [2] defines these points at 10% and 40% of M_{max}, which are herein

indicated with the subscripts 1 and 2, respectively. E_{GLT} then reads as:

$$E_{GLT} = \frac{12\,(\ell + 2e)}{bh^3} \cdot \frac{M_2 - M_1}{2\,(\phi_2 - \phi_1)}, \tag{5}$$

and f_b reads as:

$$f_b = \frac{6M_{max}}{bh^2}, \tag{6}$$

where the dimensions ℓ, e, b, and h can be found in Fig. 3.

3. Experimental validation and model verification

The mesh size dependency of the proposed numerical model is discussed in Section 3.1 before an experimental validation is shown in Section 3.2. Section 3.3 discusses how different dimensional ratios are considered in the present study.

3.1. Influence of mesh size

The mesh size was of relevance for the bottom half of the beam, where vertical cracking was enabled. In order to quantify the influence of the mesh size, three different discretizations were used: two, three, and four finite element layers over the lamella depth. Over the half lamella width, three, four, and five finite element layers were used, respectively. For the upper beam half, each lamella was discretized with only one element over the depth and a length of about 60 mm.

GLT beam sections with a fixed dimensional ratio of 1.5 and variable depths of 165 mm, 330 mm, 660 mm, and 1980 mm were investigated. For each strength class and depth, 50 simulations were performed and the results were combined in probability distribution functions (PDFs) fitted by maximum likelihood estimations. A normal distribution was applied for the effective MOE E_{GLT} and a log-normal distribution for the bending strength f_b.

The effective MOE E_{GLT} turned out to be independent of the mesh size (deviation of about 0.1 %). The bending strength f_b showed only a minor dependency on the mesh size (Fig. 5). The mean bending strength $f_{b,mean}$ and characteristic bending strength $f_{b,k}$ obtained with two finite element layer per lamella depth showed a difference to the finest mesh of less than 2%. The maximum deviation was determined for $f_{b,k}$, corresponding to beam sections of strength class GL30h with a depth of 660 mm (Fig. 5c). As a result, two finite element layer per lamella depth were used for all further simulations.

3.2. Experimental validation

With the herein proposed modeling approach (Section 2.2), the estimated effective MOE E_{GLT} and bending strength f_b agree well with experimental results from 40 tested GLT beams, covering two strength classes and beam sizes (Fig. 6). The results stem from an experimental study on GLT beams with well-known knot morphology presented by Kandler et al. [17]. The test setup was a four-point bending test consistent with DIN EN 408 [2], and the beams were manufactured from the same boards that served herein as basis for the virtual boards (Section 2.1). All positions of the boards within the beam layout were documented. The beams had no finger joints.

The four beam types A, B, D, and E are designated according to their strength class and number of lamellas as follows: A/T14-4, B/T22-4, D/T14-10, and E/T22-10. Ten tests were carried out for each type. The beam depth was 132 mm and 330 mm for the beams consisting of four and ten lamellas, respectively. The homogeneous beam layout made out of lamellas from strength class T14 or T22

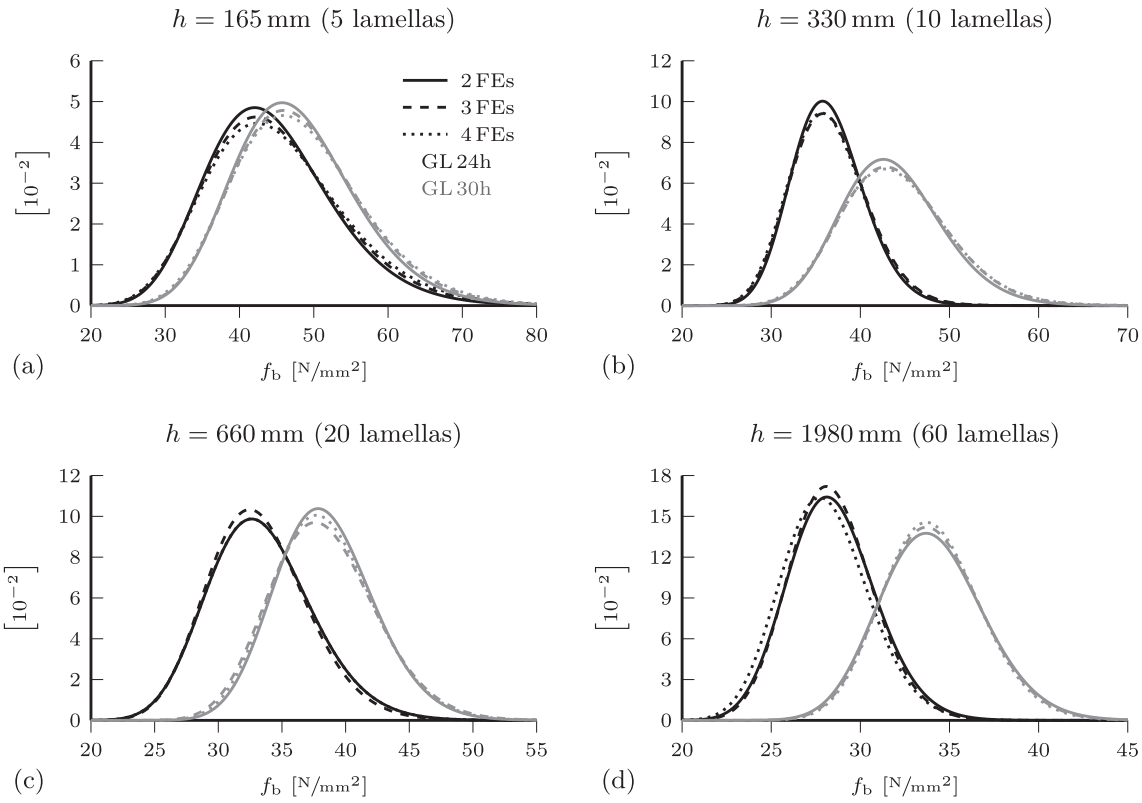

Fig. 5. Comparison of PDFs for the bending strength f_b obtained from simulations with different discretization: two, three, or four finite element layers over the lamella depth covering both strength classes and four beam section depths: (a) 165 mm, (b) 330 mm, (c) 660 mm, and (d) 1980 mm.

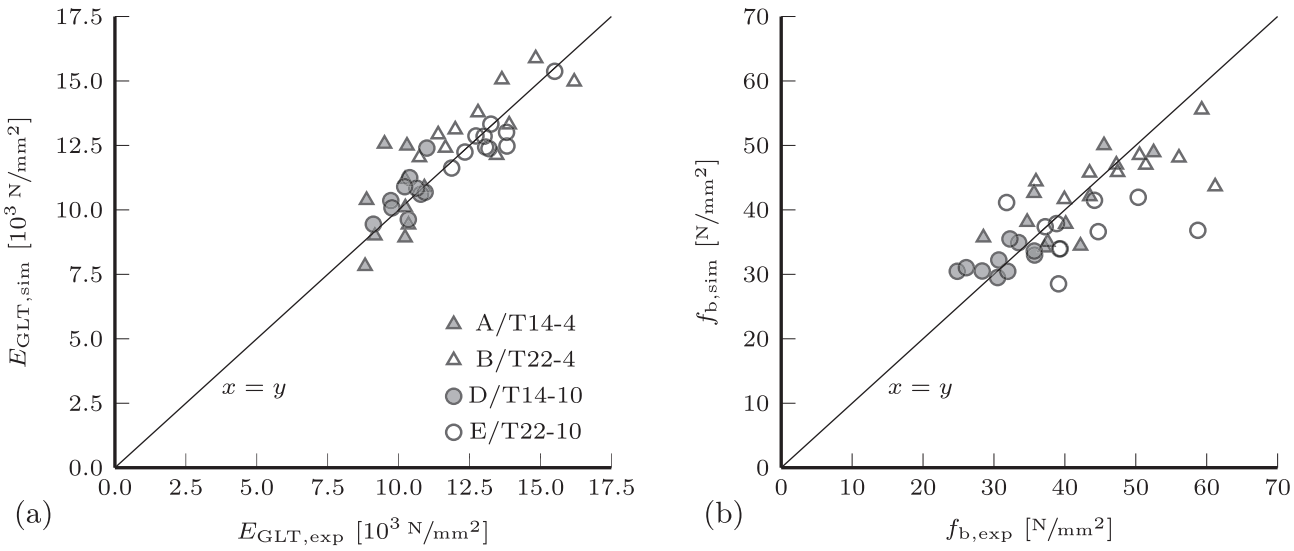

Fig. 6. Comparison of experimental results (subscript exp) to simulation results (subscript sim) for (a) the effective MOE E_{GLT} and bending strength f_b.

resulted in beams of the strength class GL24h or GL30h, respectively.

For the validation, each beam layout of the tested GLT beams was herein reconstructed within the modeled beam sections, which had the same dimensional ratio as the experiments: $\ell/h = 6.0$. The simulated effective MOE E_{GLT} (Fig. 6a) and bending strength f_b (Fig. 6b) agree well with the experimental results. The average results for each type are provided in Table 2.

3.3. Consideration of different dimensional ratios

It can be assumed that the beam length to depth ratio ℓ/h, also referred to as dimensional ratio, influences the structural response. In order to estimate the extent of this influence, 1400 simulations were carried out with modeled sections having a ratio ℓ/h of 6.0 and 4800 simulations with a ratio ℓ/h of 1.5, both ratios covered beam depths h of 165 mm, 330 mm, and 660 mm. Again, normal distributions were fitted with maximum likelihood estimations to the effective MOE E_{GLT} and log-normal distributions to the bending strength f_b.

The resulting PDFs for the three different beam depths are given in Fig. 7. For each beam depth and property, the PDFs for the two different dimensional ratios and strength classes are plotted against each other. The mean effective MOE $E_{GLT,mean}$ is hardly influenced by the dimensional ratio (Fig. 7a–c), with a maximum deviation of 2.2%. The same applies to the characteristic effective MOE $E_{GLT,k}$, which differs by a maximum of 4.6%. Thus, the dimensional ratio has only an insignificant influence on E_{GLT}.

In contrast, the bending strength f_b heavily depends on the dimensional ratio (Fig. 7d–f). This poses a problem because as the model size increases with increasing dimensional ratio, the nonlinear calculations to determine the bending strength become very time consuming. For this reason, it would be very valuable to predict the bending strength for different dimensional ratios only based on the results of the finite element models with a ratio of 1.5.

This was achieved by combining the n simulation results for the dimensional ratio of 1.5 to estimate results for larger dimensional ratios $p \times 1.5$ in the following way:

$$f_{b,i} = \min\left(f_{b,(i-1)\cdot p+1}, f_{b,(i-1)\cdot p+2}, \ldots, f_{b,(i-1)\cdot p+p}\right), \tag{7}$$

with $i \in \{1, \ldots, \lfloor n/p \rfloor\}$, where $\lfloor \cdot \rfloor$ denotes the floor function that rounds the included number to the nearest smaller integer.

This method could be roughly validated by evaluating it for $p = 4$ and comparing it to the available simulation results for the dimensional ratio of 6.0, which is shown in Fig. 8. Considering the simplicity of Eq. (7), the agreement with the simulation results is surprisingly good, with a maximum deviation of the mean bending strength of 3.3% and the characteristic bending strength of 2.2%. For this reason, this method can be used to estimate the influence of different dimensional ratios.

4. Results and discussion regarding the size effect

For addressing the size effect, an extensive simulation program covering beams in the standardized test setup [2] with depths ranging from 165 mm up to 3300 mm, corresponding to two common strength classes GL24h and GL30h, was carried out. The number of simulations performed depended on the beam size but was

Table 2
Mean values of the effective MOE E_{GLT} and the bending strength f_b of all four beam types obtained from simulations (subscript sim). $E_{GLT,rel}$ denotes the ratio of simulated over experimental results.

Type[a]	$\bar{E}_{GLT,sim}$ [N/mm^2]	$\bar{f}_{b,sim}$ [N/mm^2]	$\bar{E}_{GLT,rel}$ [–]	$\bar{f}_{b,rel}$ [–]
A	10275	39.9	1.04	1.02
B	13559	46.7	1.04	0.97
D	10619	32.1	1.03	1.05
E	12859	37.0	0.97	0.89

[a] Ten beams of each type.

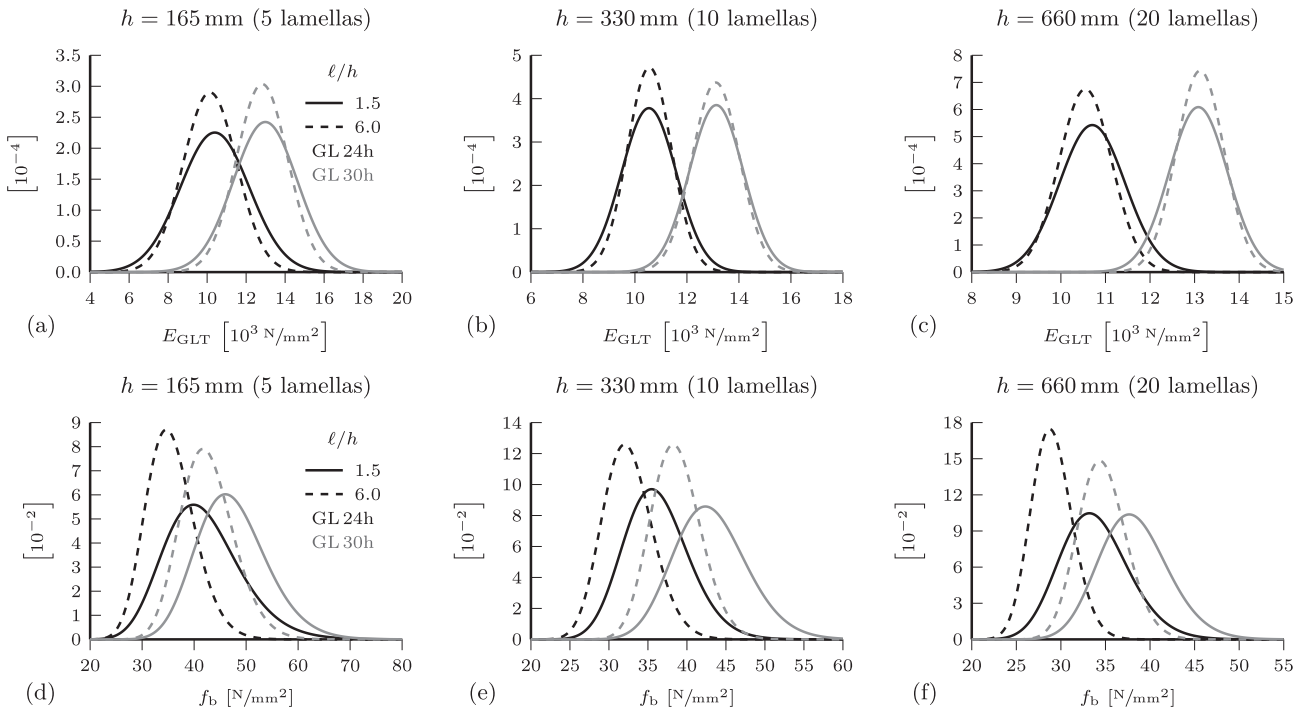

Fig. 7. Comparison of PDFs for (a–c) the effective MOE E_{GLT} and (d–f) the bending strength f_b obtained from simulations with the dimensional ratios of 6.0 or 1.5 covering both strength classes for three beam depths: 165 mm, 330 mm, and 660 mm.

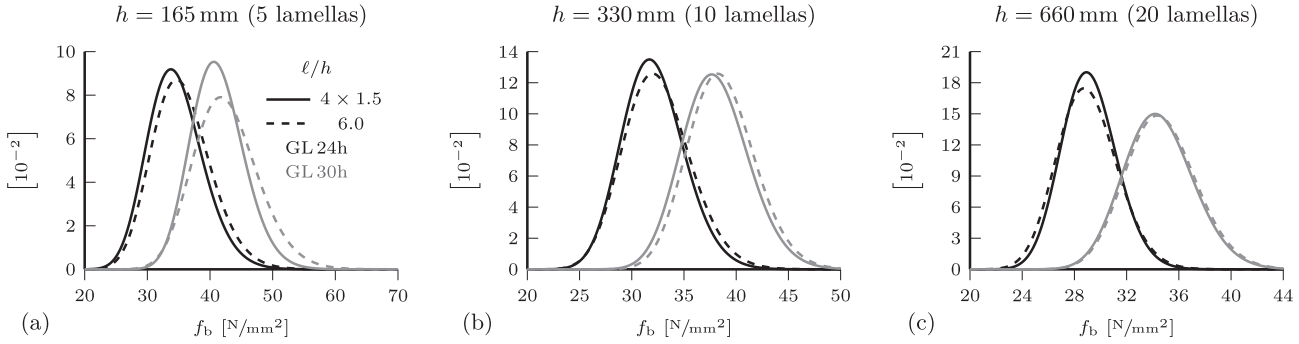

Fig. 8. Comparison of PDFs for the bending strength f_b obtained from simulations with the dimensional ratios of 6.0 or 4 × 1.5 covering both strength classes for three beam depths: (a) 165 mm, (b) 330 mm, and (c) 660 mm.

the same for both strength classes (Table 3). All models had a dimensional ratio of 1.5 using the modeling approach presented in Section 2.2 and were generated by random assembly of the 140 virtually reconstructed wooden boards of each strength class described in Section 2.1.

Table 3
Studied beam depths with the corresponding number of lamellas and simulations.

Depth h [mm]	Lamellas [–]	Sample size[a] [–]
165	5	1600
330	10	400
660	20	400
1320	40	400
1980	60	300
2640	80	200
3300	100	200

[a] For each strength class with $\ell/h = 1.5$.

Fig. 9 shows exemplarily one model for each beam size and the corresponding obtained failure mechanism. Finally, the approach provided the effective MOE E_{GLT} and bending strength f_b according to Eqs. (5) and (6), respectively. For different absolute lengths of a beam section with specific depth (different dimensional ratios), the corresponding bending strengths f_b were obtained according to Section 3.3.

This section is structured as follows: First, the choice of suitable PDFs based on a sufficient number of simulations is discussed in Section 4.1. The influence of considering plasticity in regions with compressive stresses is briefly outlined in Section 4.2. Section 4.3 and Section 4.4 address the size effect with respect to E_{GLT} and f_b, respectively. Finally, the influence of the beam length on f_b for each beam depth is presented in Section 4.5.

4.1. Choice of probability distribution functions and sample sizes

First, the suitability of different two-parameter PDFs was visually assessed by quantile–quantile (Q–Q) plots, i.e., normal and

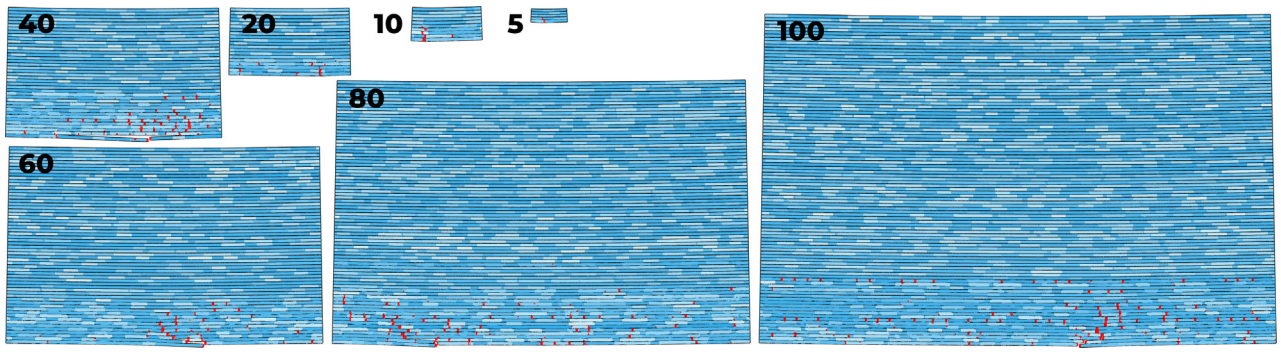

Fig. 9. Exemplary layout and failure mechanisms of simulated GLT beam sections with a dimensional ratio of 1.5 for all seven depths, built by five to 100 lamellas. The effective longitudinal MOE E_{L} is illustrated in *blue* with increasing values from light to dark shading and vertical cracks are highlighted in *red*.

log-normal distributions for the effective MOE E_{GLT} and log-normal and Weibull distributions for the bending strength f_{b}. Maximum likelihood estimations fitted the distribution parameters. The visually best fit was used for all further investigations. Second, the change of the mean and characteristic values was analyzed with increasing sample size, up to the maximum number of simulations for a certain beam depth, given in Table 3. All those results are shown in detail for the whole simulation program in Appendix A in Fig. A1–A6. The results are summarized in Fig. 10.

The simulation results of the effective MOE E_{GLT} fitted best to the normal distribution. From as little as about 20% of the carried out simulations, the mean and the characteristic value are relatively constant and the deviation from the final value is less than 2% (Fig. 10a).

To the bending strengths f_{b} obtained from simulations, the log-normal distribution fitted best. Two different lengths of each beam depth were separately studied with a dimensional ratio of 1.5 and 4×1.5. From about 65% of the sample size, characteristic values over- or underestimate the final result by less than 2% (Fig. 10b, c). Generally, the mean value shows a smaller deviation from the final result than the characteristic value.

4.2. Influence of considering plasticity

Considering plasticity in compressive stress regions changes the stress distribution over the cross-section. According to beam theory, under bending and for a material with ideal elastic-plastic behavior the linear distributed tensile stresses increase with increasing plastic zones for compressive stresses over a cross-section. For this reason, consideration of plastic deformations should reduce the effective GLT bending strength. To identify this influence, we compared the same beam section layout with and without considering plasticity.

The plastic deformations mainly affected beams of smaller depth and of the higher strength class (Fig. 11). However, the characteristic bending strength $f_{\mathrm{b,k}}$ of all three beam sizes is affected by less than 1% using the ratio ℓ/h of 1.5 . A greater influence was observed for the simulations reaching higher bending strengths. The results using the ratio ℓ/h of 4×1.5 had an even smaller influence. Frese [25] found a slightly more pronounced influence using the *Karlsruher Calculation Model*. This could be caused by the different modeling strategies, where their strategy models failure even more brittle.

4.3. Size effect on the effective MOE

The effective MOEs obtained by the simulation program clearly demonstrate, for both strength classes, that with increasing beam size the variation reduces and the mean value stays essentially constant (Fig. 12a,b). A normal distribution (Section 4.1) was fitted to the simulation results to determine characteristic values. The following paragraphs discuss the accuracy of the obtained mean values and the consequences of the variation.

In contrast to the mean values provided by DIN EN 14080 [1], the mean values derived from the simulations result in an underestimation for the lower strength class of about 7% and for the higher one of about 3% (Table 4). Considering all model assumptions, including the virtual reconstruction of the boards, these deviations are acceptable and rather small.

The changing variation causes the characteristic value to depend on the beam size, which conflicts with the constant characteristic value provided by DIN EN 14080 [1]. The proportion factor $k_{\mathrm{h},E}$ describes the characteristic to mean value ratio to address this

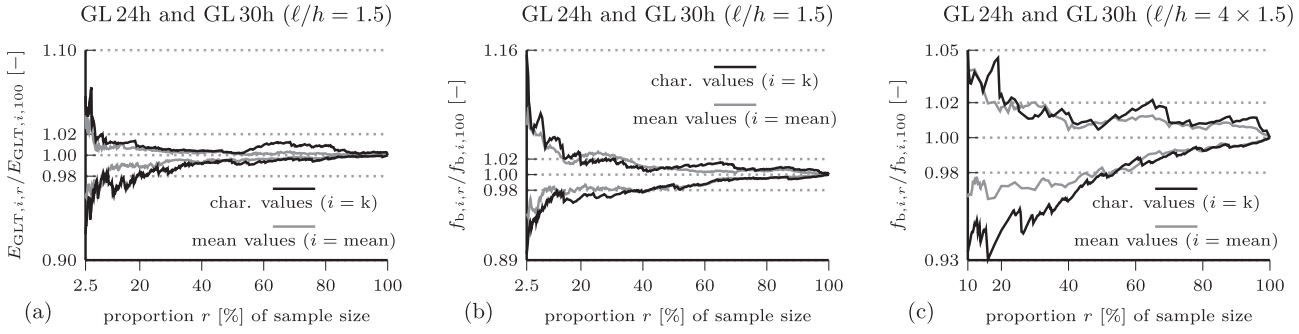

Fig. 10. Evolution of characteristic and mean values as envelope curves, including all beam depths and both strength classes, depending on the proportion r of the sample size for (a) the effective MOE E_{GLT} based on normal distributions and (b,c) the bending strength f_{b} based on log-normal distributions from results with a dimensional ratio of 1.5 and 4×1.5, respectively.

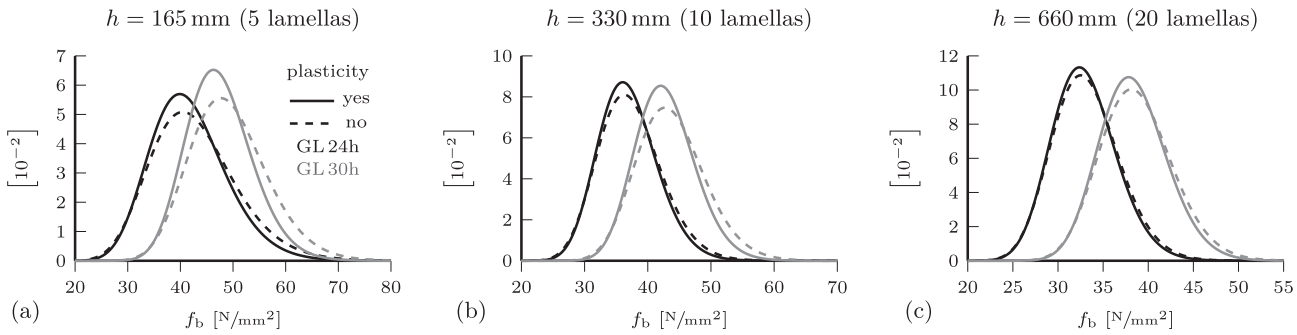

Fig. 11. Comparison of the bending strength distributions obtained from simulations with and without considered plasticity for the dimensional ratio of 1.5 three beam depths: (a) 165 mm, (b) 330 mm, and (c) 660 mm.

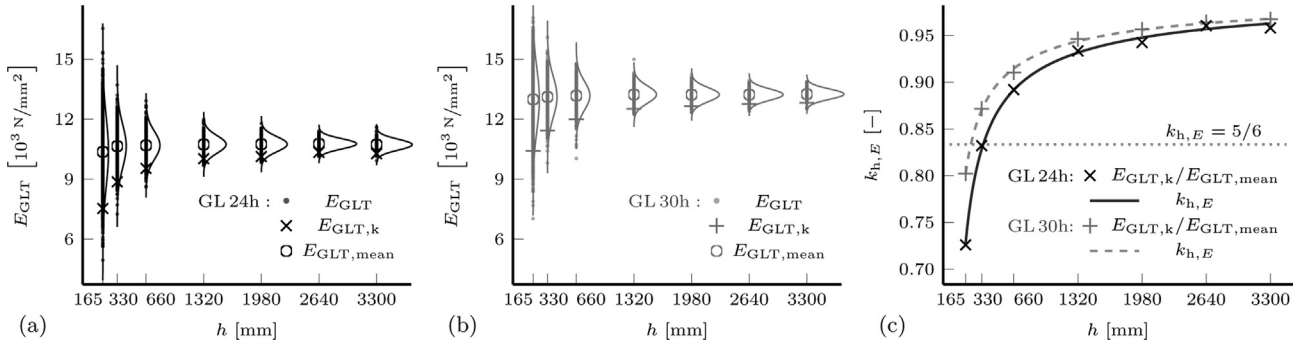

Fig. 12. Effective MOE E_{GLT} values and normal distributions obtained from simulations with the beam depth h and a dimensional ratio of 1.5 for strength classes (a) GL24h and (b) GL30h, which are used to derive (c) the proportional factor $k_{h,E}$.

Table 4
Mean longitudinal MOE $E_{0,g,mean}$ according to DIN EN 14080 [1] compared to the mean effective MOE $E_{GLT,mean}$ from the performed simulations (sim) and the experiments (exp) presented in Section 3.2.

Strength class	$E_{0,g,mean}$ [N/mm²]	$E^{sim}_{GLT,mean}$ [N/mm²]	$E^{exp}_{GLT,mean}$ [N/mm²]
GL24h	11500	10666	10075
GL30h	13600	13168	13159

effect. Generally, our simulations of beams with a depth over 330 mm result in higher proportion factors than the defined constant factor of 5/6 in [1] (Fig. 12c).

A suitable functional description of the proportional factor $k_{h,E}$ (Fig. 12c) was found based on the size effect concept according to Eq. (1) from [3]:

$$k_{h,E} = 1 - m_0 \cdot \left(\frac{600}{h}\right)^{1/m_1}, \tag{8}$$

where m_0 and m_1 are parameters depending on the strength class. Based on the simulation results, the parameters of Eq. (8) were determined with the least squares method, for both strength classes:

$$\text{GL24h}: \begin{cases} m_0 & = 0.1156 \\ m_1 & = 1.5078 \end{cases}. \tag{9}$$

$$\text{GL30h}: \begin{cases} m_0 & = 0.0906 \\ m_1 & = 1.6523 \end{cases}. \tag{10}$$

For beams of the reference depth ($h_{ref} = 600$ mm), Eq. (8) results in a proportion factor $k_{h,E}$ of 88% and 91% in conjunction with the parameters from Eqs. (9) and (10), respectively. Experimental tests in the literature [13–15] suggest no evident influence of the beam size. However, the considered beam depths are restricted to about 300 mm and 600 mm.

4.4. Size effect on the bending strength

The effective bending strengths, obtained by our simulations, decreased for both strength classes with increasing beam size (Fig. 13a,b). This size effect becomes even more obvious when looking at the trend of the characteristic strength values normalized to the characteristic strength of the reference beam depth of 600 mm (Fig. 13c). The log-normal distribution (Section 4.1) provided the basis to derive mean and characteristic values. The following paragraphs are dedicated to the functional description of the characteristic strength in conjunction with the factor k_h, which is commonly used to describe the size effect.

The size effect on the characteristic bending strength $f_{b,k}$ can be analytically described by the concept of DIN EN 1995-1-1 [3], introduced in Eq. (1). Herein, we use the same concept to analytically describe our simulation results. We modify the characteristic reference bending strength $f_{b,k,ref}$ by k_h for a beam with depth h as follows:

$$f_{b,k} = f_{b,k,ref} \cdot k_h = m_2 \cdot \left(\frac{600}{h}\right)^{1/m_3}, \tag{11}$$

where m_2 is a parameter which equals $f_{b,k,ref}$ and the decrease of k_h is controlled by the reciprocal of m_3. In the concept of DIN EN 1995-1-1 [3], m_2 is the characteristic bending strength $f_{m,g,k}$ of the corresponding strength class, and the parameter m_3 is identified as being 10 from Eq. (1).

The simulation results of $f_{b,k,ref}$ for GL24h and GL30h overestimate the values provided by DIN EN 14080 [1] by about 7% and 4%, respectively. For the derivation of $f_{b,k,ref}$ (m_2), the parameters m_2

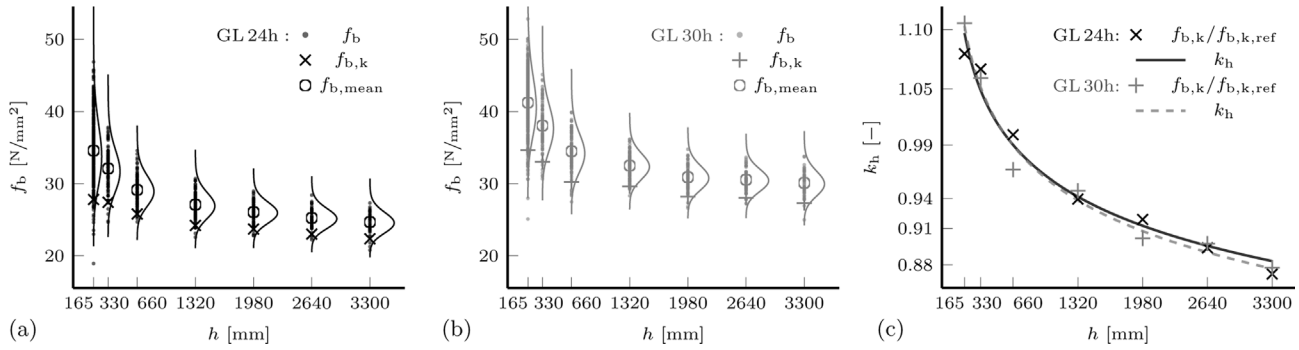

Fig. 13. Bending strength f_b values and distributions obtained from simulations with the beam depth h and a dimensional ratio of 4 × 1.5 for strength classes (a) GL24h and (b) GL30h, which are used to derive (c) the factor k_h commonly describing the size effect.

and m_3 on the right-hand side of Eq. (11) were fitted to our simulation results employing the least squares method:

$$\text{GL24h}: \begin{cases} m_2 & = 25.74 \quad \text{N/mm}^2 \\ m_3 & = 13.50 \end{cases}, \tag{12}$$

$$\text{GL30h}: \begin{cases} m_2 & = 31.23 \quad \text{N/mm}^2 \\ m_3 & = 12.69 \end{cases}. \tag{13}$$

The label of a strength class matches the characteristic bending strength provided in [1], with GL24h and GL30h referring to 24 N/mm² and 30 N/mm², respectively. The modification of the characteristic strength offered by [1] to account for a lamella depth diverging from 40 mm was omitted.

Our predicted size effect quantifies the strength decrease with increasing beam size. As a result, the characteristic bending strengths $f_{b,k}$ of beams with a depth of 3300 mm experience a decrease of about 12% compared to $f_{b,k,ref}$ (Fig. 13c), which applies to both strength classes. The concept of k_h in DIN EN 1995-1-1 [3] considers only beam sizes smaller than the reference size. For such beams, the herein obtained distribution of k_h agrees well with the one defined by Eq. (1) from [3]. Furthermore, the established k_h describes the strength decrease of beam sizes greater than the reference size.

In comparison to the literature results, the decreasing trend agrees with the results presented by Frese and Blaß [24]. In [24], a reduction of about 18% for beams with 3000mm depth was predicted by employing the *Karlsruher Calculation Model*. The findings of Fink et al. [32] were contradictory, generally observing no size effect for beams with a depth in the range of 320 mm to 1200 mm using a probabilistic approach. However, these variations can be explained by different model assumptions, especially with regard to the global failure criterion. A detailed description of the different models, a comprehensive comparison to our modeling approach, and an in-depth analysis of our simulation results including the different failure modes will be presented in a subsequent publication.

4.5. Influence of the dimensional ratio

For the effective MOE, the comparison of different beam lengths suggests only a minor influence of the dimensional ratio (Fig. 7a–c). In contrast, the bending strength seems to depend heavily on the dimensional ratio (Fig. 7d–f). Thus, an appropriate formulation is needed to determine realistic bending strengths for varying dimensional ratios.

To be able to analyze this dependency in an efficient way, we have proposed in Section 3.3 a procedure only using the simulation results of the model with a dimensional ratio of 1.5. With this procedure, we estimated the bending strengths of GLT sections with seven different depths and five different lengths to depth ratios ℓ/h, ranging from 1.5 to 9.0.

The obtained characteristic bending strengths $f_{b,k,h,\ell/h}$ were then normalized by the result $f_{b,k,h,6.0}$ of the corresponding beam depth h with a ratio ℓ/h of 6.0 (4 × 1.5). This normalized value is denoted as $k_{\ell/h}$, and it is plotted for the individual simulated beam depths h in Fig. 14. There, the influence of different beam lengths, based on the five ratios, is illustrated for all beam depths individually. The beam length for a specific ratio is thus different for each beam depth.

Generally, for each beam depth, the bending strength decreases with increasing dimensional ratio (beam length). This effect is more pronounced for smaller beam depths, especially smaller than 660 mm. Above 660 mm the factor $k_{\ell/h}$ stays almost constant with increasing beam depth h for each dimensional ratio. This effect can be described quite adequately with the general relation proposed by Colling [48] (Fig. 14, horizontal lines), based on Weibull's theory [4], reading:

$$k_h = \left(\frac{V_{ref}}{V}\right)^{1/m_4}. \tag{14}$$

A volume V is composed of its length ℓ, width b, and depth h. Specification of Eq. (14) for beams with a constant width, dimensional reference ratio of 6.0, and reference depth of 600 mm leads to:

$$k_h = \left(\frac{6.0 \cdot 600^2}{\ell/h \cdot h^2}\right)^{1/m_4}, \tag{15}$$

where ℓ/h denotes the specific dimensional ratio with the length ℓ and depth h. Finally, the factor k_h can be normalized by dividing

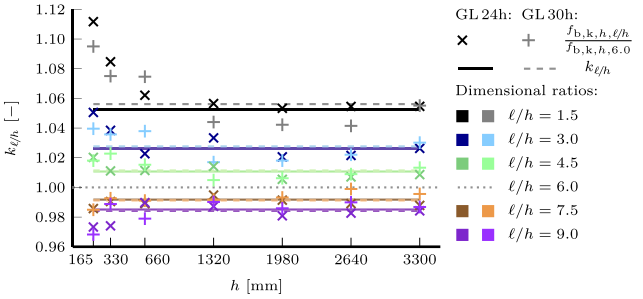

Fig. 14. Comparison of the normalized values $k_{\ell/h}$, which denote the difference of the characteristic bending strength $f_{b,k}$ for different dimensional ratios (beam section lengths) in reference to the dimensional reference ratio ($\ell/h = 6.0$) of each individual beam depth h. The scatters refer to the simulated results obtained by using the procedure proposed in Section 3.3. The horizontal lines are based on Weibull's strength theory [4] obtained by Eq. (16).

Eq. (15) with itself specified for the dimensional reference ratio $\ell/h = 6.0$, giving the factor $k_{\ell/h}$:

$$k_{\ell/h} = \left(\frac{6.0 \cdot 600^2}{\ell/h \cdot h^2}\right)^{1/m_4} / \left(\frac{6.0 \cdot 600^2}{6.0 \cdot h^2}\right)^{1/m_4} = \left(\frac{6.0}{\ell/h}\right)^{1/m_4}. \quad (16)$$

The parameter m_4 can be determined based on the realized simulations (Fig. 13), where $m_4 = 2 \cdot m_3$ for the corresponding strength class from Eqs. (12) and (13). The relation comes from considering the beam length and depth in Eqs. (15) in comparison to Eq. (11), where only the depth is used.

5. Conclusion and outlook

We proposed a modeling approach to predict the effective MOE and bending strength of GLT beams, taking into account essential mechanical effects. At the same time, the approach was efficient enough to perform extensive simulation programs. Based on 8840 simulations, covering two different strength classes, beam depths from 165 mm to 3300 mm, and two different depth to beam lengths, the size effect regarding stiffness and strength properties could be identified and discussed. The normal and log-normal distributions proved suitable for describing the effective MOE and the bending strength distribution obtained from simulations. The number of simulations required to achieve reliable distributions decreased with increasing beam depth. The consideration of plastic deformations in regions with high compressive stresses had no significant impact on the predicted characteristic strength values.

Regarding the effective MOE E_{GLT}, the following conclusion can be drawn:

- For both investigated strength classes, the characteristic stiffness values increased with increasing beam depth. However, the mean values were nearly constant, independent of the beam depth. As a result, the coefficient of variation decreased with increasing beam depth, questioning the depth-independent ratio of characteristic to mean value from DIN EN 14080 [1].

Regarding the bending strength f_b, the following conclusions are drawn:

- Based on a comprehensive simulation program, the size effect could be determined qualitatively as well as quantitatively for beam depths ranging from 165 mm to 3300 mm. For the characteristic strength values a continuous decrease was observed, up to about 12% strength reduction compared to the reference depth of 600 mm. However, the variation of obtained strength values significantly decreased with increasing beam depths. All these effects applied to both investigated strength classes.
- The influence of the length of the GLT beam or dimensional ratio ℓ/h, respectively, can be estimated with sufficient accuracy using an analytical formula according to Colling [48], especially for beam depths larger than 660 mm. This was validated by means of simulation results and a concept to extent these results to arbitrary beam lengths.

Further research, based on the same data, is going to focus on the failure mechanisms observed for different beam sizes. This includes analyzing the number of lamellas contributing to the failure process and the influence of employing different global failure criteria. Such knowledge benefits the development of future modeling approaches.

In the future, the constant fracture energies will be replaced by section-wise constant ones, which can be achieved by detailed numeric simulations of the knot sections applying the so-called phase field method for fracture presented by Pech et al. [49,50]. Due to the three-dimensional modeling, variable material properties over the width can be implemented in the approach easily. Additionally, it is easy to adapt the approach to investigate the failure behavior of GLT beam sections under tensile loads.

Furthermore, we suggest research on the decreasing coefficient of variation for increasing beam depths for both examined material properties, i.e., the effective MOE and the bending strength. This is important for developing future holistic design concepts with a constant failure probability.

6. Data availability

The raw/processed data required to reproduce these findings cannot be shared at this time as the data also forms part of an ongoing study.

Data availability

Data will be made available on request.

Declaration of Competing Interest

The authors declare that they have no known competing financial interests or personal relationships that could have appeared to influence the work reported in this paper.

Acknowledgement

This research was funded in whole, or in part, by the Austrian Science Fund (FWF) [Y1093–N30]. For the purpose of open access, the author has applied a CC BY public copyright license to any Author Accepted Manuscript version arising from this submission. The authors also acknowledge gratefully the support by the Forest-Value project InnoCrossLam.

Appendix A. Material property distributions for different beam depths

In this appendix, we present the simulation-based PDFs for the effective MOE E_{GLT} and the bending strength f_b for each investigated beam depth and strength class. The distributions were fitted by employing maximum likelihood estimations. The Hazen method [51] determined the theoretical quantiles in the Q–Q plots to visually assess the more suitable fit. For determining the required number of simulations (sample size) regarding a certain beam depth, the change of the characteristic values with an increasing sample size is shown. The characteristic values were chosen because they are subject to greater variation than the mean values. Appendix A.1 presents the results regarding the effective MOE E_{GLT} and Appendix A.2 regarding the bending strength f_b.

A.1. Effective MOE distributions

The normal and log-normal distributions of the effective MOE E_{GLT} were compared for each strength class, GL24h (Fig. A1) and GL30h (Fig. A2). Table A1 provides the individual values of all presented PDFs. We found that the normal distribution represents a more suitable fit compared to the log-normal distribution. Further, the observed change of the characteristic value for an increasing number of considered simulations was generally independent from the selected distribution.

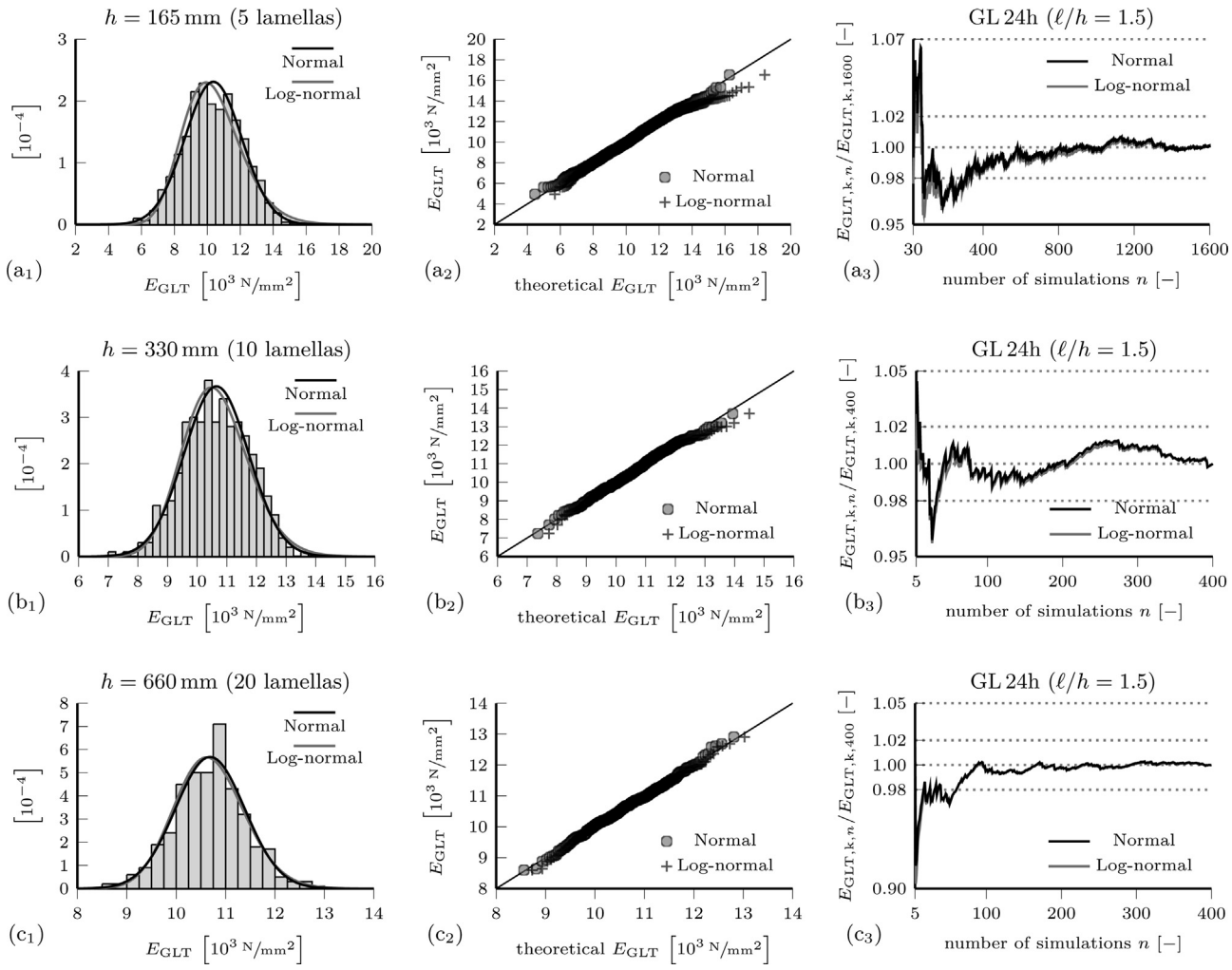

Fig. A1. The effective MOE E_{GLT} obtained from simulations of beam sections with different depths (a–g), a dimensional ratio of 1.5, and belonging to strength class GL24h. For each depth, the histogram with normal and log-normal distributions, the Q–Q plot, and the relative change of the characteristic values for an increasing number of considered results n are illustrated and referred to by subscripts 1–3, respectively.

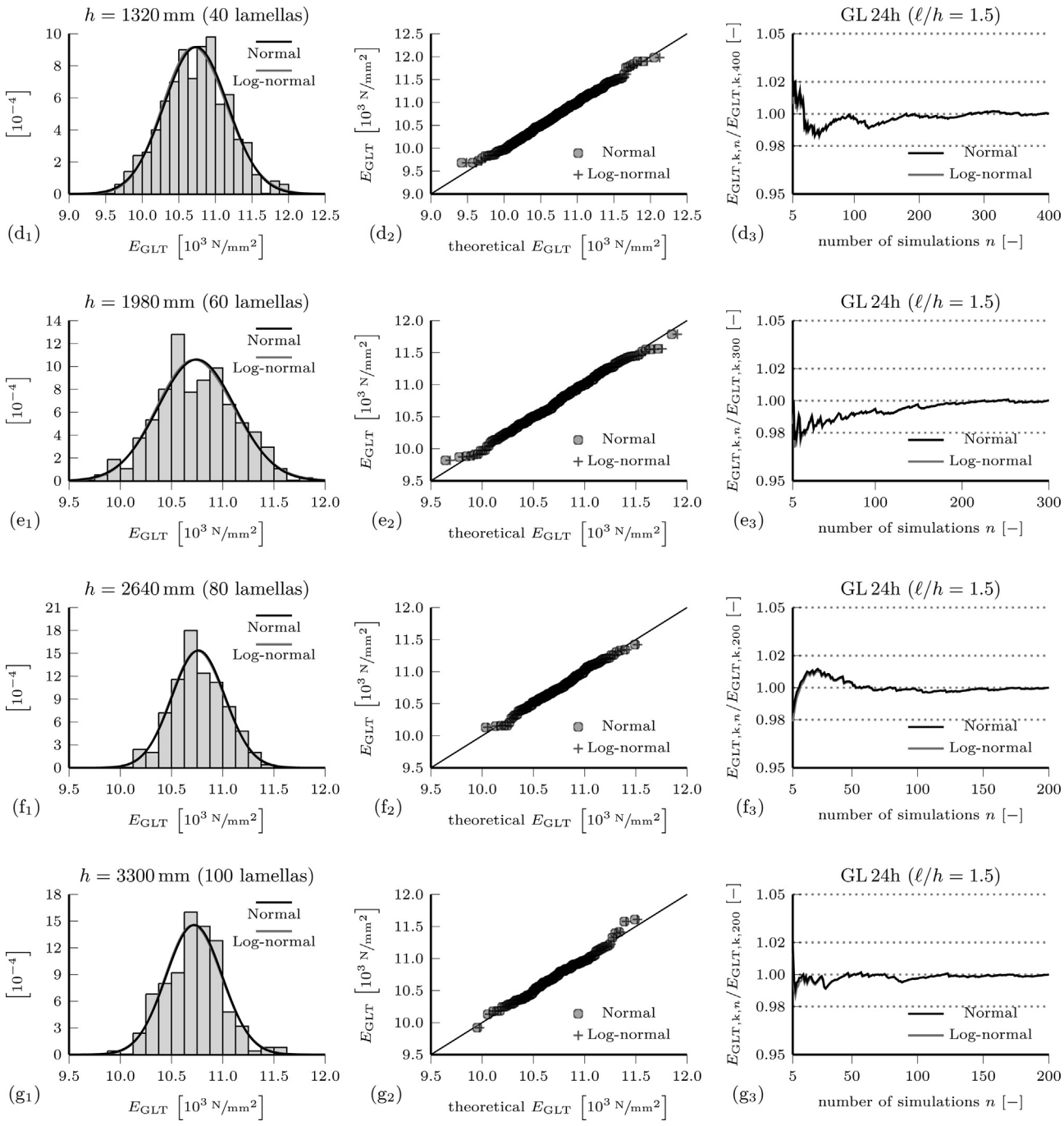

Fig. A1 (*continued*)

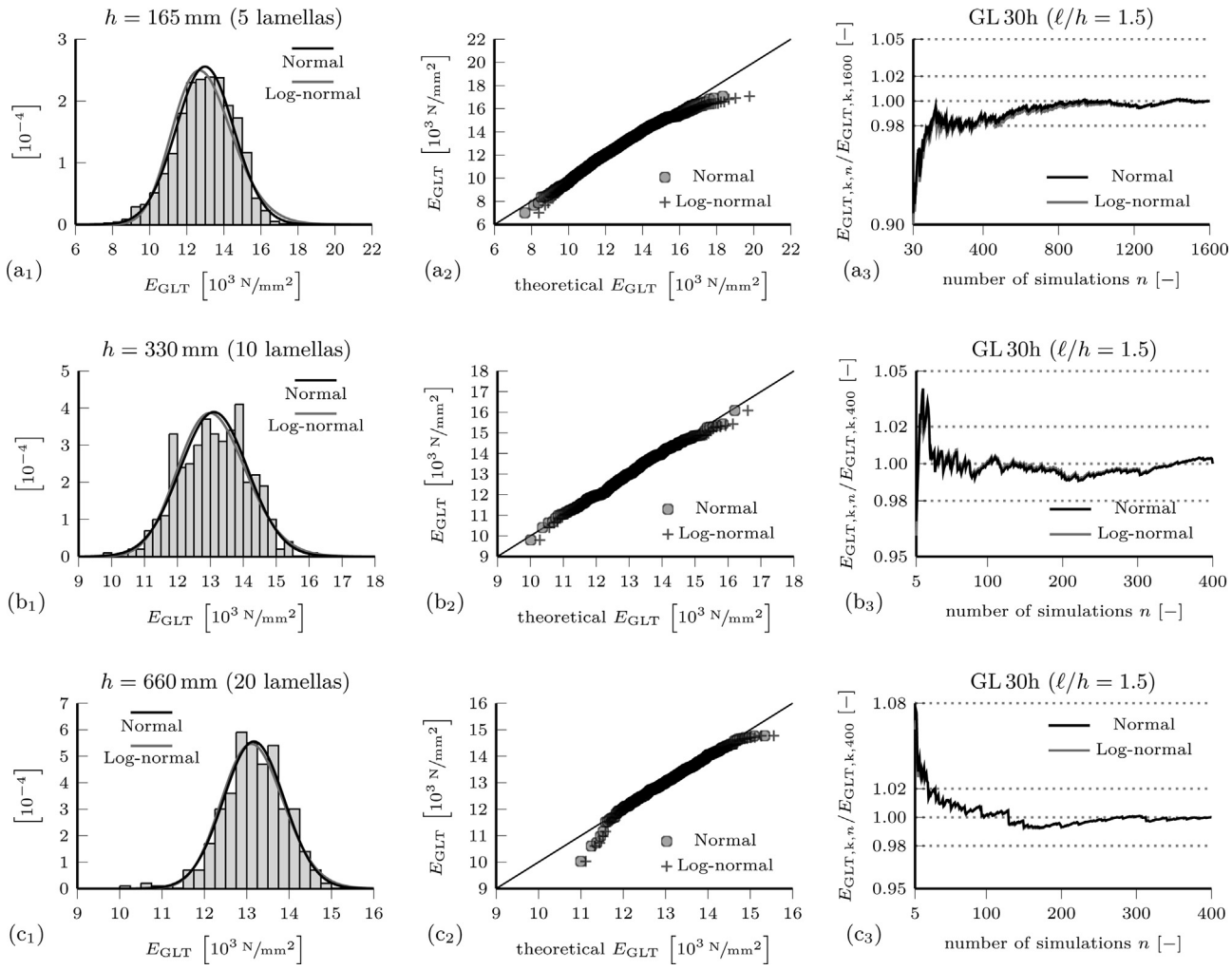

Fig. A2. The effective MOE E_{GLT} obtained from simulations of beam sections with different depths (a–g), a dimensional ratio of 1.5, and belonging to strength class GL30h. For each depth, the histogram with normal and log-normal distributions, the Q–Q plot, and the relative change of the characteristic values for an increasing number of considered results n are illustrated and referred to by subscripts 1–3, respectively.

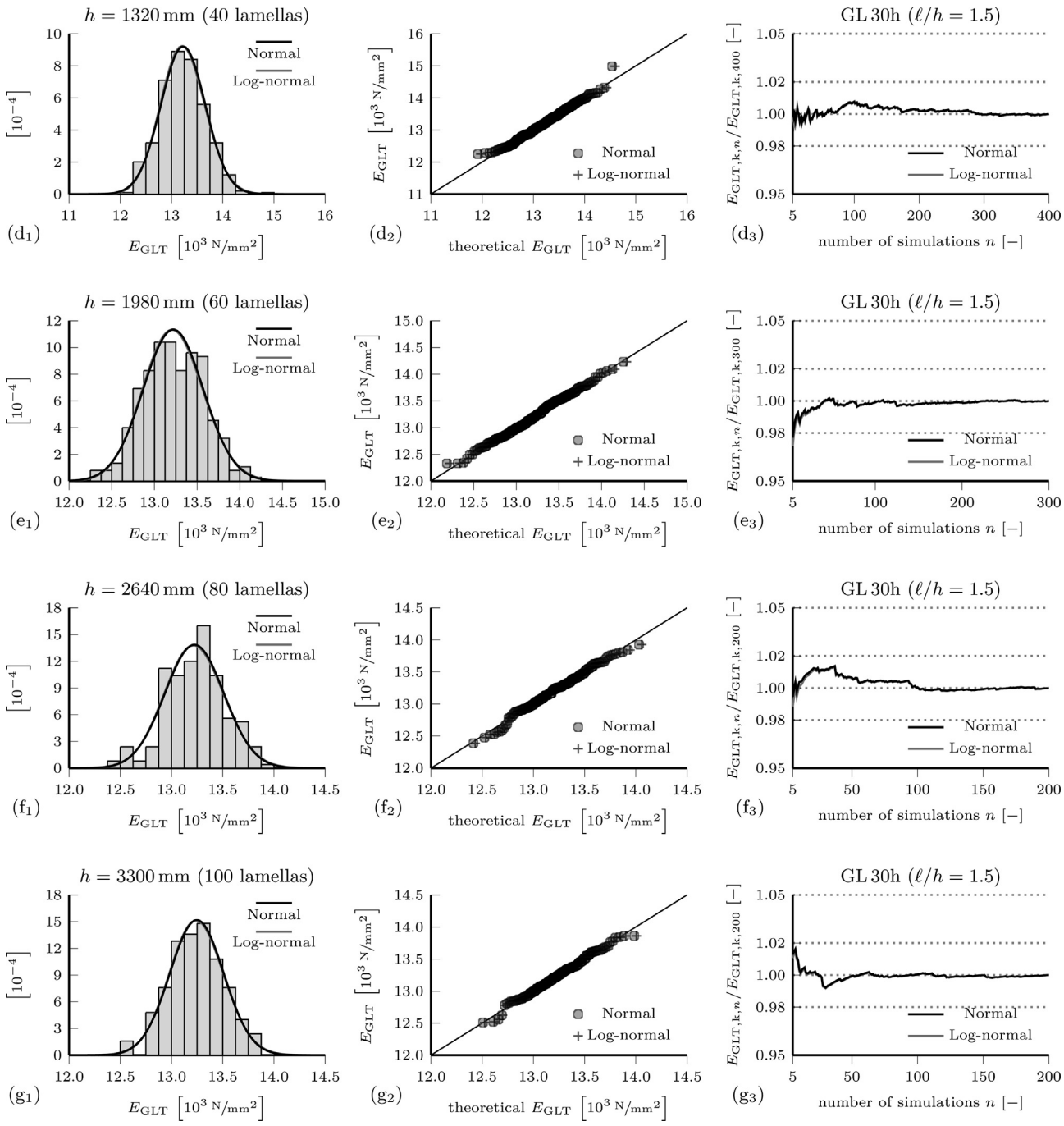

Fig. A2 (*continued*)

Table A1
Distributions of the effective MOE E_{GLT} for GLT beam sections with depth h and a dimensional ratio of 1.5.

Strength class	Depth h	Normal distribution			Log-normal distribution		
		5% quantile	mean	CV[a]	5% quantile	mean	CV[a]
	[mm]	[N/mm²]	[N/mm²]	[–]	[N/mm²]	[N/mm²]	[–]
GL24h	165	7523	10363	0.1666	7694	10367	0.1736
	330	8860	10648	0.1021	8928	10649	0.1041
	660	9530	10686	0.0657	9562	10686	0.0663
	1320	10019	10734	0.0405	10032	10734	0.0406
	1980	10126	10745	0.0350	10136	10746	0.0351
	2640	10337	10764	0.0241	10341	10764	0.0242
	3300	10271	10722	0.0256	10276	10722	0.0256
GL30h	165	10415	12983	0.1203	10489	12986	0.1256
	330	11423	13109	0.0782	11472	13109	0.0793
	660	11987	13168	0.0546	11999	13169	0.0556
	1320	12514	13227	0.0328	12526	13227	0.0328
	1980	12642	13220	0.0266	12649	13220	0.0267
	2640	12750	13224	0.0218	12753	13224	0.0219
	3300	12815	13247	0.0198	12818	13247	0.0199

[a] Coefficient of variation.

A.2. Bending strength distributions

The log-normal and Weibull distributions of the bending strength f_b were compared for each strength class based on results with a dimensional ratio of 1.5 (Fig. A3 for GL24h and Fig. A4 for GL30h) and of 4×1.5 (Fig. A5 for GL24h and Fig. A6 for GL30h). The individual values of all presented distributions are provided in Table A2 and Table A3 for the dimensional ratio of 1.5 and

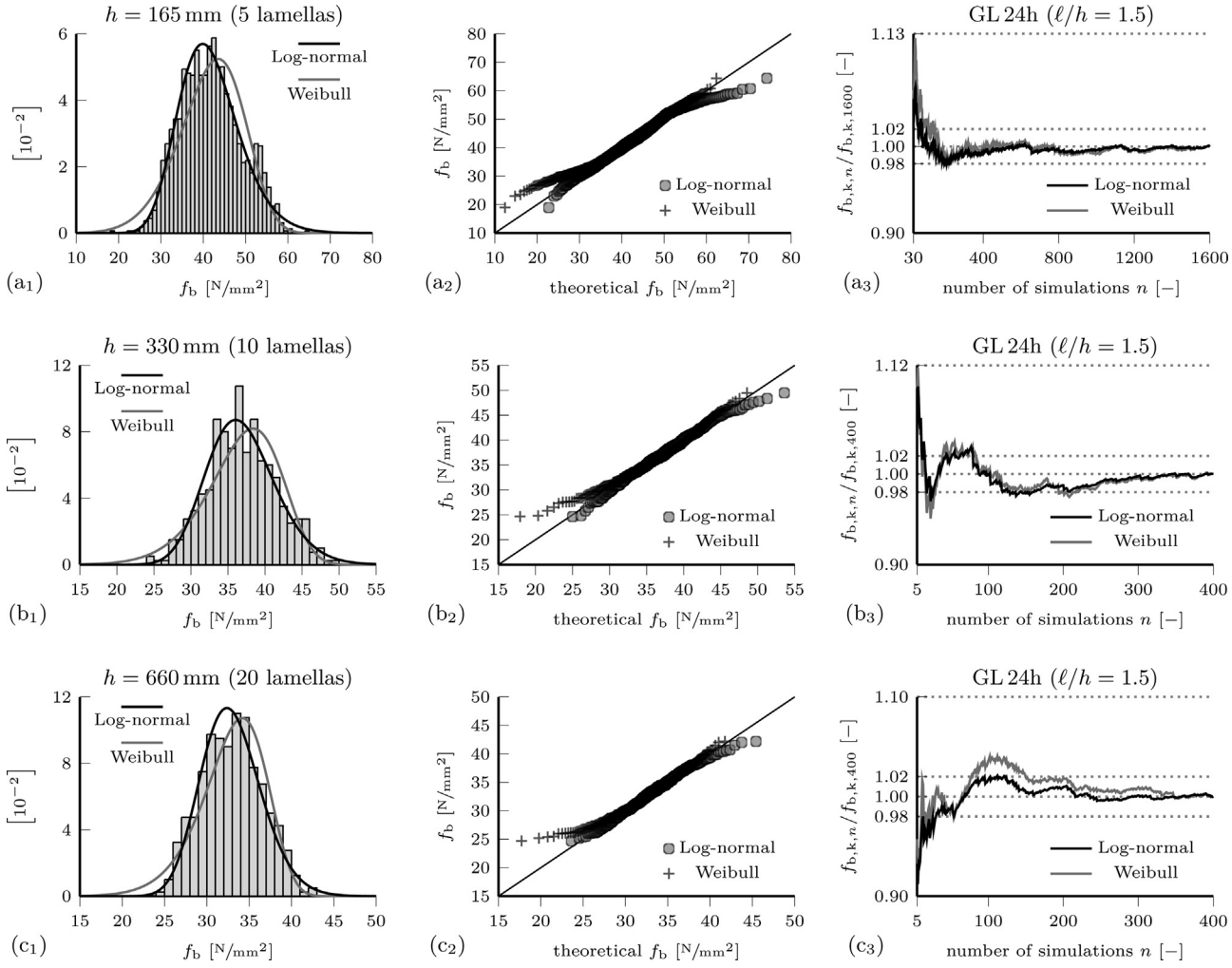

Fig. A3. The bending strength f_b obtained from simulations of beam sections with different depths (a–g), a dimensional ratio of 1.5, and belonging to strength class GL24h. For each depth, the histogram with normal and log-normal distributions, the Q–Q plot, and the relative change of the characteristic values for an increasing number of considered results n are illustrated and referred to by subscripts 1–3, respectively.

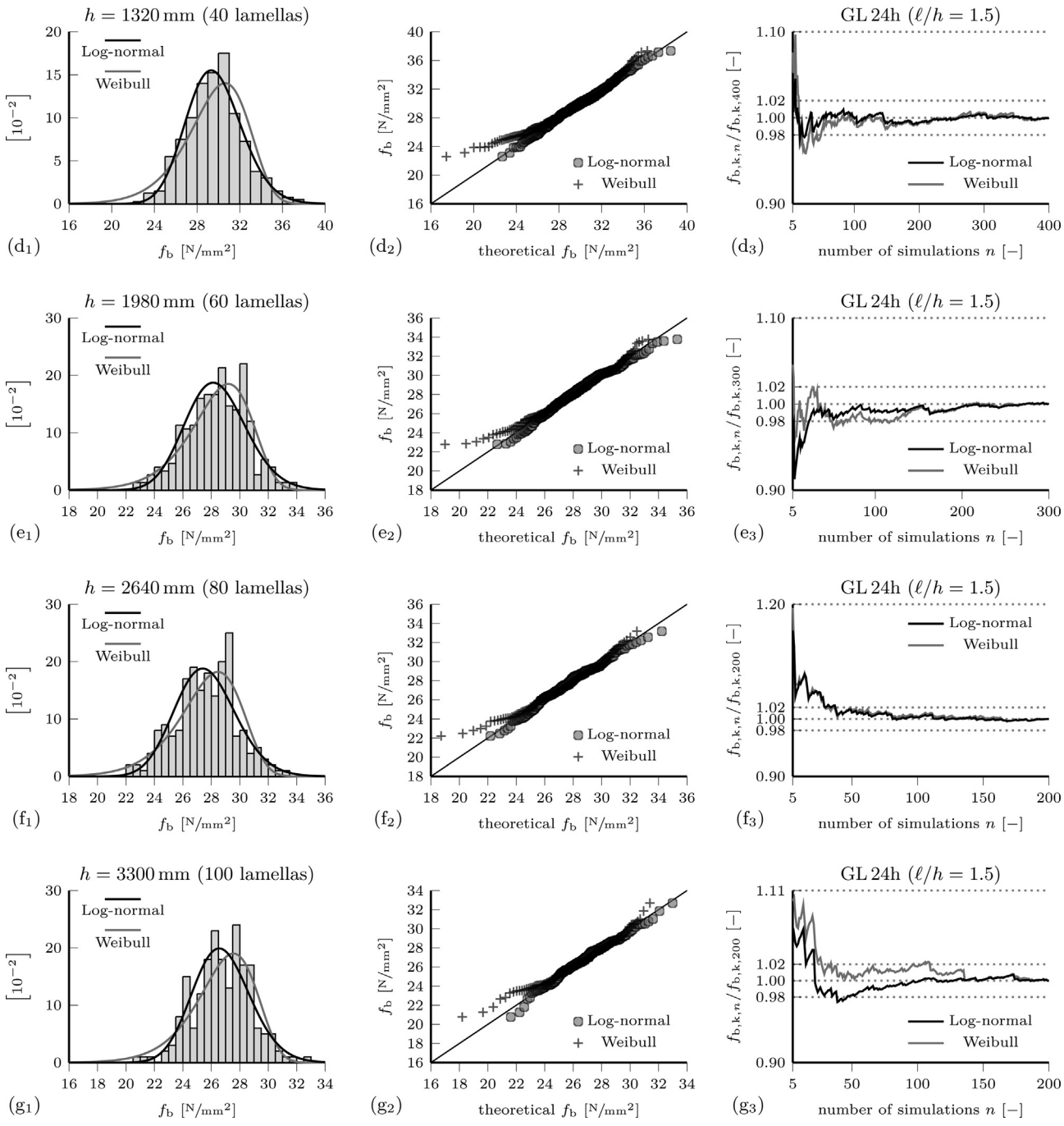

Fig. A3 (*continued*)

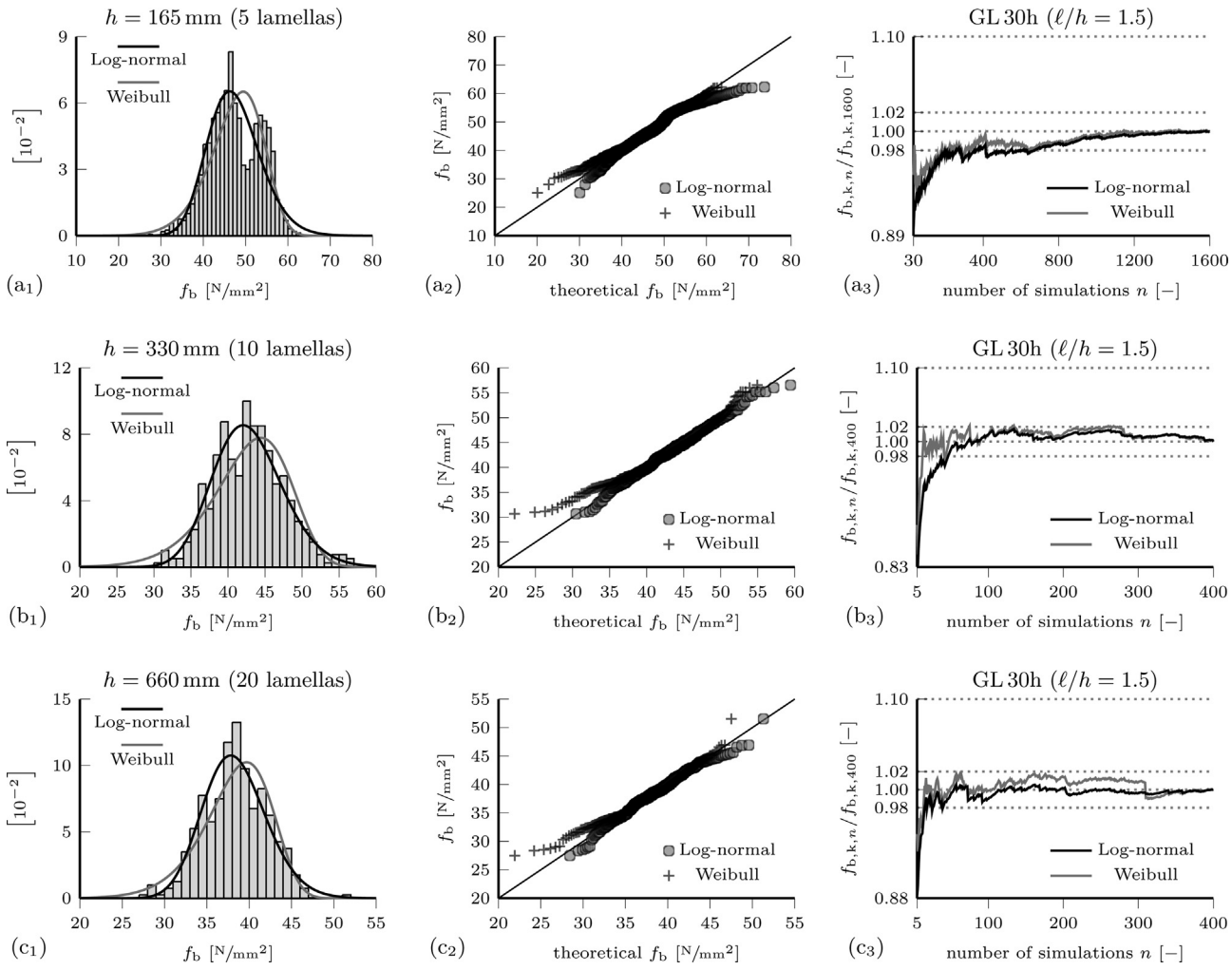

Fig. A4. The bending strength f_b obtained from simulations of beam sections with different depths (a–g), a dimensional ratio of 1.5, and belonging to strength class GL30h. For each depth, the histogram with normal and log-normal distributions, the Q–Q plot, and the relative change of the characteristic values for an increasing number of considered results n are illustrated and referred to by subscripts 1–3, respectively.

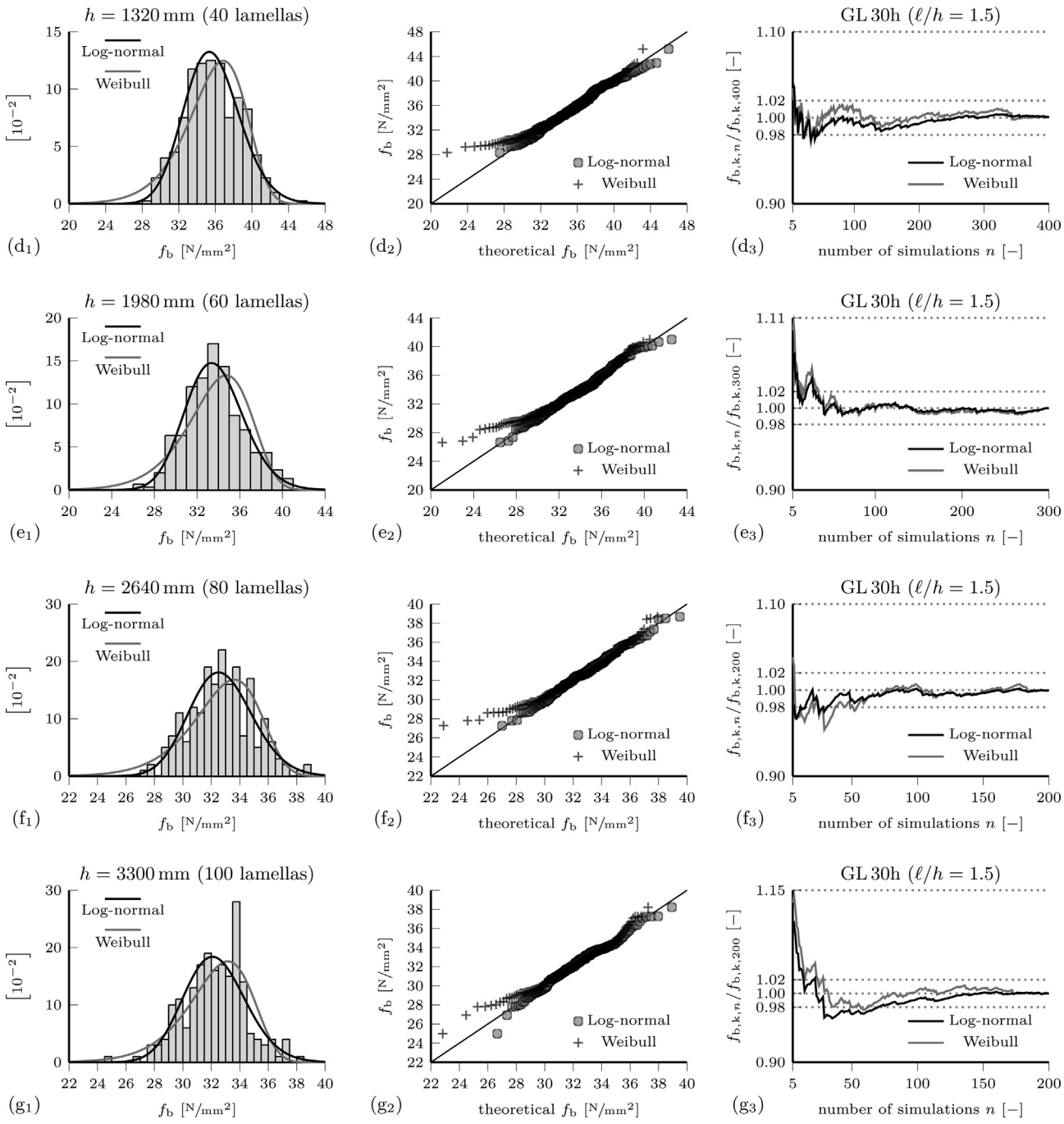

Fig. A4 (*continued*)

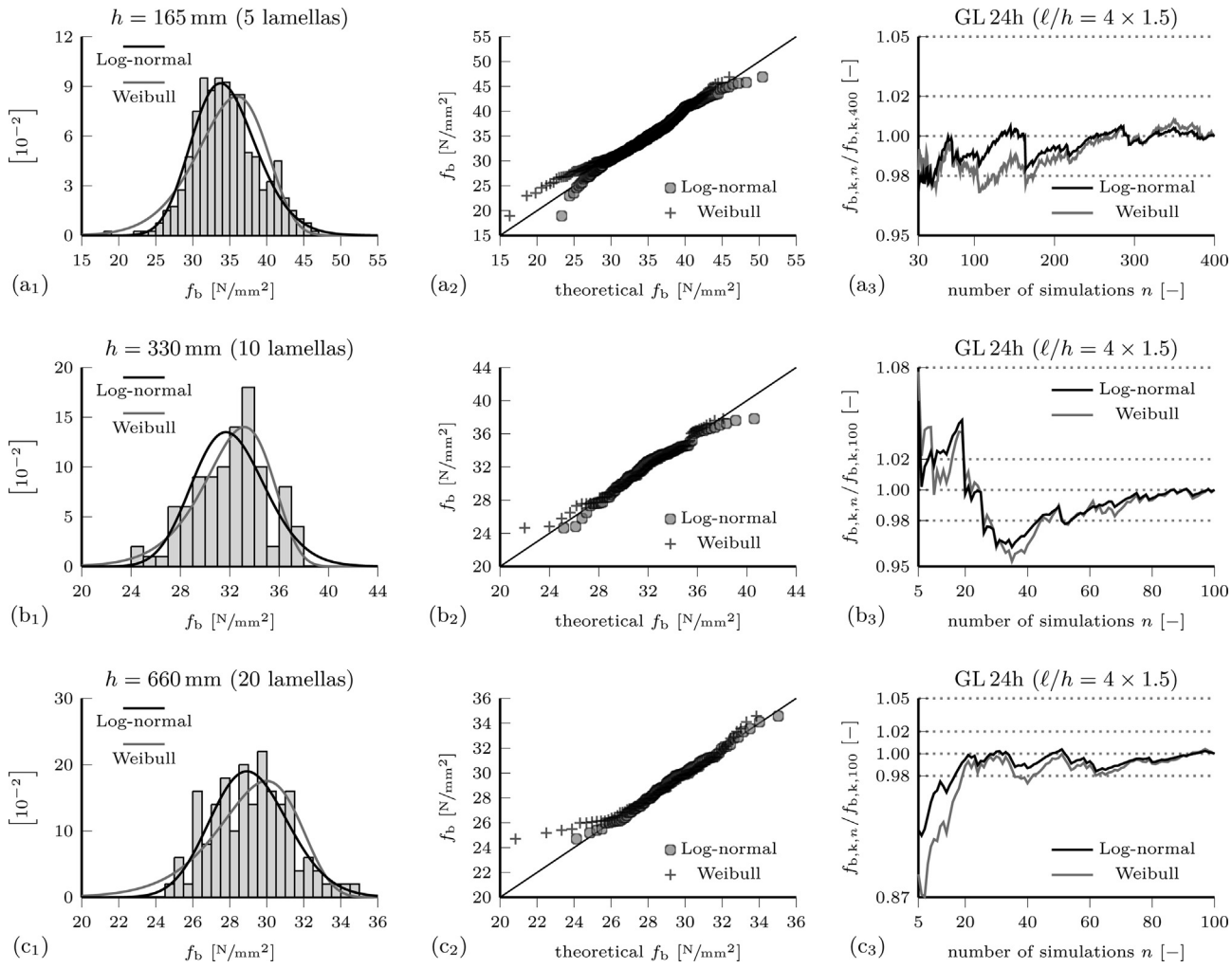

Fig. A5. The bending strength f_b obtained from simulations of beam sections with different depths (a–g), a dimensional ratio of 4×1.5, and belonging to strength class GL24h. For each depth, the histogram with normal and log-normal distributions, the Q–Q plot, and the relative change of the characteristic values for an increasing number of considered results n are illustrated and referred to by subscripts 1–3, respectively.

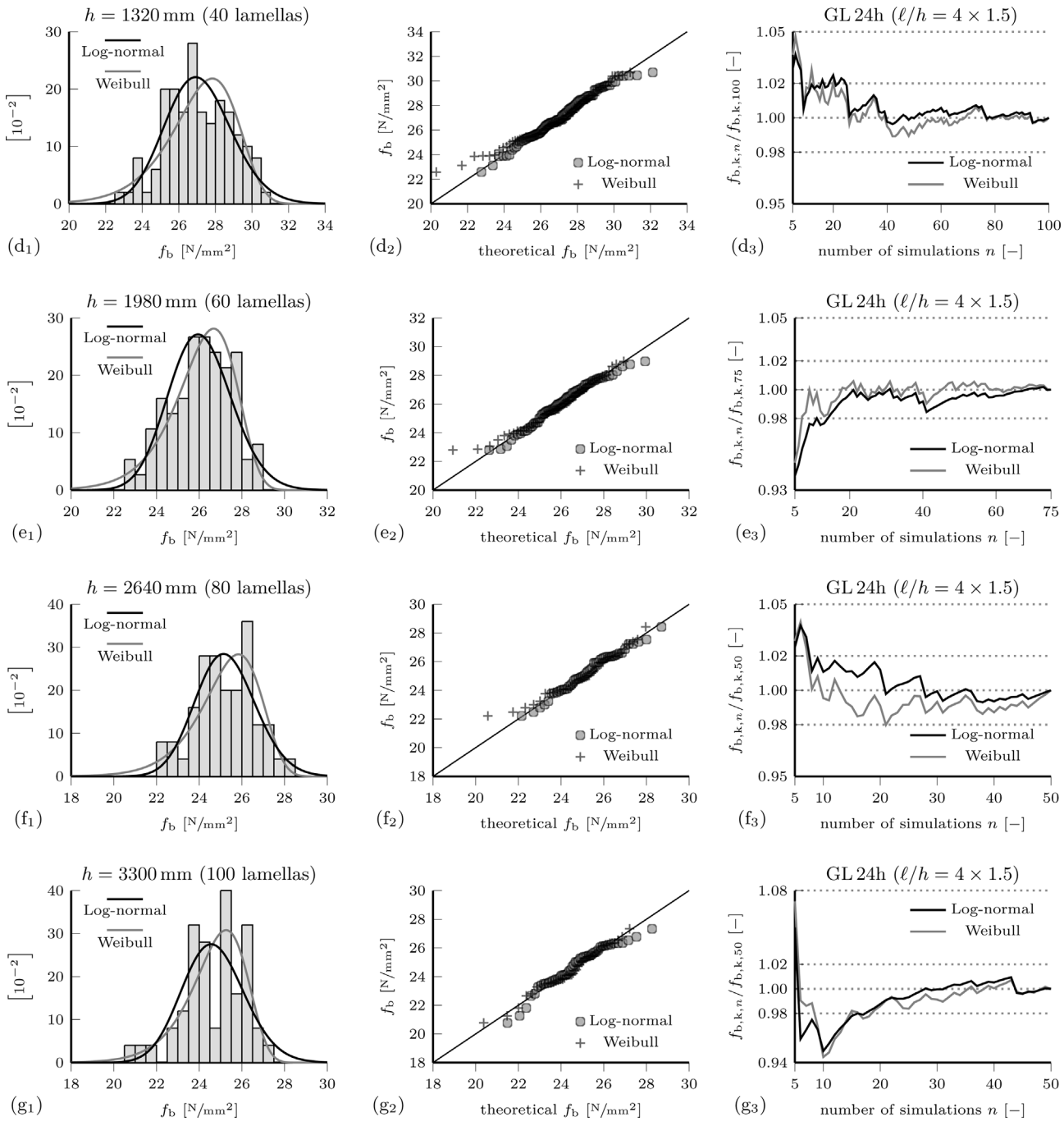

Fig. A5 (*continued*)

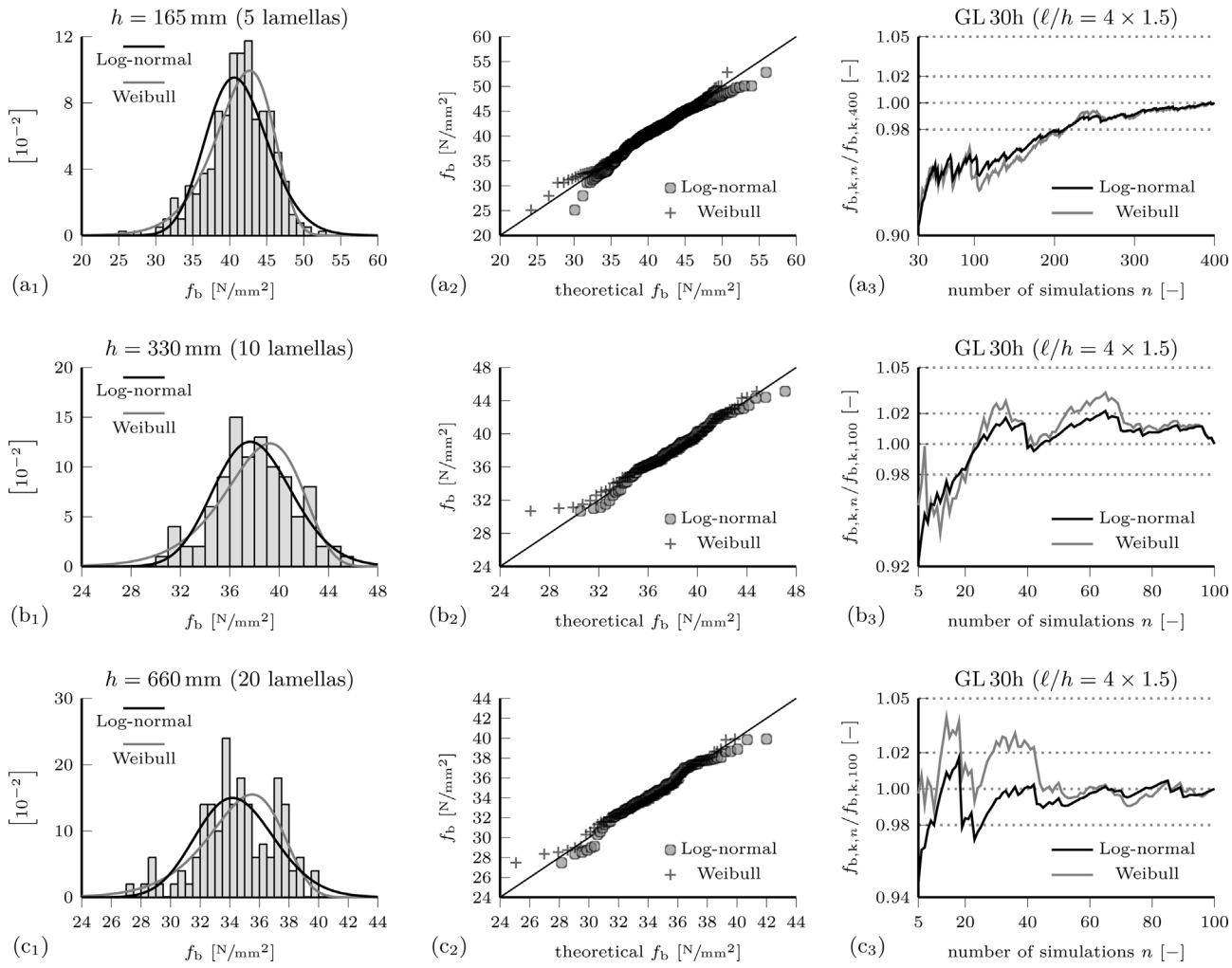

Fig. A6. The bending strength f_b obtained from simulations of beam sections with different depths (a–c), a dimensional ratio of 4×1.5, and belonging to strength class GL30h. For each depth, the histogram with normal and log-normal distributions, the Q–Q plot, and the relative change of the characteristic values for an increasing number of considered results n are illustrated and referred to by subscripts 1–3, respectively.

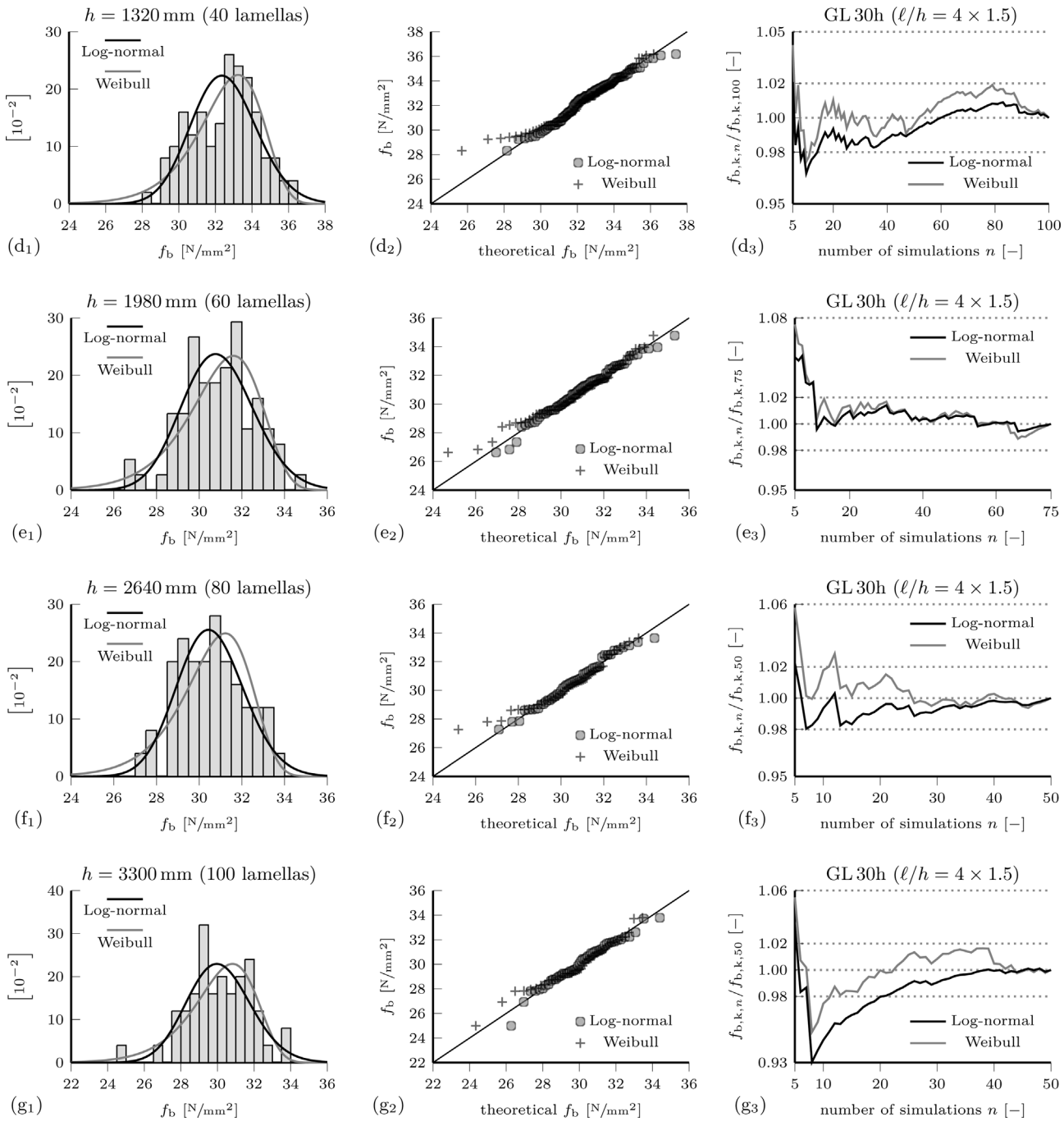

Fig. A6 (*continued*)

4×1.5, respectively. We found that the log-normal distribution represents a more suitable fit compared to the Weibull distribution. Further, the observed change of the characteristic value for an increasing number of considered simulations was generally more sensitive for the Weibull distribution than the log-normal distribution.

Table A2
Distributions of the bending strength f_b for GLT beam sections with depth h and a dimensional ratio of 1.5.

Strength class	Depth h	Log-normal distribution			Weibull distribution		
		5% quantile	mean	CV[a]	5% quantile	mean	CV[a]
	[mm]	[N/mm²]	[N/mm²]	[–]	[N/mm²]	[N/mm²]	[–]
GL24h	165	30.92	41.72	0.1743	27.91	41.62	0.1855
($\ell/h = 1.5$)	330	29.76	36.90	0.1265	27.58	36.80	0.1385
	660	27.41	32.94	0.1085	25.68	32.86	0.1201
	1320	25.59	29.66	0.0875	23.95	29.54	0.1035
	1980	24.98	28.37	0.0757	23.97	28.31	0.0833
	2640	24.27	27.64	0.0774	23.18	27.57	0.0867
	3300	23.59	26.78	0.0754	22.49	26.70	0.0858
GL30h	165	37.95	47.49	0.1316	35.79	47.43	0.1355
($\ell/h = 1.5$)	330	35.49	42.82	0.1108	32.83	42.66	0.1268
	660	32.53	38.37	0.0978	30.64	38.25	0.1090
	1320	30.94	35.71	0.0851	29.28	35.61	0.0971
	1980	29.40	33.68	0.0809	27.63	33.57	0.0965
	2640	29.21	32.73	0.0678	27.84	32.63	0.0798
	3300	28.84	32.29	0.0675	27.61	32.21	0.0774

[a] Coefficient of variation.

Table A3
Distributions of the bending strength f_b for GLT beam sections with depth h and a dimensional ratio of 4×1.5.

Strength class	Depth h	Log-normal distribution			Weibull distribution		
		5% quantile	mean	CV[a]	5% quantile	mean	CV[a]
	[mm]	[N/mm²]	[N/mm²]	[–]	[N/mm²]	[N/mm²]	[–]
GL24h	165	27.81	34.59	0.1281	25.52	34.46	0.1437
($\ell/h = 4 \times 1.5$)	330	27.43	32.10	0.0931	26.42	32.07	0.0960
	660	25.81	29.15	0.0725	24.50	29.06	0.0854
	1320	24.22	27.10	0.0670	23.35	27.06	0.0744
	1980	23.72	26.07	0.0566	23.12	26.05	0.0607
	2640	23.01	25.26	0.0557	22.32	25.22	0.0621
	3300	22.37	24.69	0.0590	22.01	24.68	0.0586
GL30h	165	34.66	41.25	0.1028	33.30	41.18	0.1046
($\ell/h = 4 \times 1.5$)	330	33.01	38.06	0.0844	31.56	37.98	0.0922
	660	30.27	34.49	0.0777	29.27	34.45	0.0817
	1320	29.64	32.50	0.0551	28.80	32.46	0.0610
	1980	28.21	30.90	0.0547	27.34	30.85	0.0616
	2640	28.05	30.56	0.0513	27.20	30.51	0.0586
	3300	27.33	30.11	0.0580	26.49	30.06	0.0643

[a] Coefficient of variation.

References

[1] DIN EN 14080, Holzbauwerke – Brettschichtholz und Balkenschichtholz – Anforderungen; Deutsche Fassung EN 14080:2013, Standard, DIN, Berlin, Germany, 2013.

[2] DIN EN 408, Holzbauwerke – Bauholz für tragende Zwecke und Brettschichtholz – Bestimmung einiger physikalischer und mechanischer Eigenschaften; Deutsche Fassung EN 408:2010+A1:2012, Standard, DIN, Berlin, Germany, 2012.

[3] DIN EN 1995-1-1, Eurocode 5: Bemessung und Konstruktion von Holzbauten – Teil 1–1: Allgemeines – Allgemeine Regeln und Regeln für den Hochbau; Deutsche Fassung EN 1995-1-1:2004 + AC:2006 + A1:2008, Standard, DIN, Berlin, Germany, 2010.

[4] W. Weibull, A statistical theory of the strength of materials, Handlingar Nr. 151, Ingeniörsvetenskapsakademiens, Generalstabens litografiska anstalts förlag, Stockholm, Sweden, 1939.

[5] L. Blank, G. Fink, R. Jockwer, A. Frangi, Quasi-brittle fracture and size effect of glued laminated timber beams, Eur. J. Wood Wood Prod. 75 (2017) 667–681, https://doi.org/10.1007/s00107-017-1156-0.

[6] M. Brunetti, M. Nocetti, B. Pizzo, F. Negro, G. Aminti, P. Burato, C. Cremonini, R. Zanuttini, Comparison of different bonding parameters in the production of beech and combined beech-spruce CLT by standard and optimized tests methods, Constr. Build. Mater. 265 (2020) 120168, https://doi.org/10.1016/j.conbuildmat.2020.120168.

[7] T. Wang, Y. Wang, R. Crocetti, M. Wålinder, Influence of face grain angle, size, and moisture content on the edgewise bending strength and stiffness of birch plywood, Mater. Des. 223 (2022) 111227, https://doi.org/10.1016/j.matdes.2022.111227.

[8] C. Tapia, S. Aicher, Survival analysis of tensile strength variation and simulated length–size effect along oak boards, J. Eng. Mech. 148 (2022) 04021130, https://doi.org/10.1061/(ASCE)EM.1943-7889.0002006.

[9] P. Nallathambi, B.L. Karihaloo, B.S. Heaton, Various size effects in fracture of concrete, Cem. Concr. Res. 15 (1985) 117–126, https://doi.org/10.1016/0008-8846(85)90016-X.

[10] A. Dönmez, M. Rasoolinejad, Z.P. Bažant, Size effect on FRP external reinforcement and retrofit of concrete structures, J. Compos. Constr. 24 (2020) 04020056, https://doi.org/10.1061/(ASCE)CC.1943-5614.0001070.

[11] Y. Zhang, H. Li, A. Abdelhady, J. Yang, H. Wang, Effects of specimen shape and size on the permeability and mechanical properties of porous concrete, Constr. Build. Mater. 266 (2021) 121074, https://doi.org/10.1016/j.conbuildmat.2020.121074.

[12] W. Luo, J.-L. Le, M. Rasoolinejad, Z.P. Bažant, Coefficient of variation of shear strength of RC beams and size effect, J. Eng. Mech. 147 (2021) 04020144, https://doi.org/10.1061/(ASCE)EM.1943-7889.0001879.

[13] R.H. Falk, K.H. Solli, E. Aasheim, The performance of glued laminated beams manufactured from machine stress graded Norwegian spruce, Meddelelse 77, Norsk Treteknisk Institutt, Oslo, Norway, 1992.

[14] E. Aasheim, K.H. Solli, Size factor of Norwegian glued laminated beams, in: Proceedings of the International Council for Research and Innovation in Building and Construction, Paper CIB-W18/28-12-2, Copenhagen, Denmark, 1995.

[15] R. Pischl, G. Schickhofer, C. Seiner, A. Steinberger, E. Gehri, R. Mauritz, Entwicklung leistungsfähiger Holzleimbauteile: Zusammenfassender Bericht zum FFF-Forschungsprojekt, FFF-Forschungsprojekt, Graz/A – Zürich/CH – Wien/A, 1995.

[16] G. Fink, J. Kohler, A. Frangi, Bending tests on glued laminated timber beams with well-known material properties: Test report, Technical Report,

ETH Zurich, Zurich, Switzerland (2013), https://doi.org/10.3929/ethz-a-009950793.
[17] G. Kandler, M. Lukacevic, J. Füssl, Experimental study on glued laminated timber beams with well-known knot morphology, Eur. J. Wood Wood Prod. 76 (2018) 1435–1452, https://doi.org/10.1007/s00107-018-1328-6.
[18] G. Fink, P. Stadelmann, A. Frangi, Bending test on large-scale GLT beams with well-known beam setup using machine grading indicator, Int. Wood Prod. J. 12 (2021) 258–266, https://doi.org/10.1080/20426445.2021.1969166.
[19] J. Ehlbeck, F. Colling, R. Görlacher, Einfluß keilgezinkter Lamellen auf die Biegefestigkeit von Brettschichtholzträgern, Holz als Roh- und Werkstoff 43 (1985) 333–337, https://doi.org/10.1007/BF02607817.
[20] J. Ehlbeck, F. Colling, R. Görlacher, Einfluß keilgezinkter Lamellen auf die Biegefestigkeit von Brettschichtholzträgern, Holz als Roh- und Werkstoff 43 (1985) 369–373, https://doi.org/10.1007/BF02607906.
[21] J. Ehlbeck, F. Colling, R. Görlacher, Einfluß keilgezinkter Lamellen auf die Biegefestigkeit von Brettschichtholzträgern, Holz als Roh- und Werkstoff 43 (1985) 439–442, https://doi.org/10.1007/BF02612470.
[22] F. Colling, Tragfähigkeit von Biegeträgern aus Brettschichtholz in Abhängigkeit von den festigkeitsrelevanten Einflussgrößen, Ph.D. thesis, Universität Karlsruhe, Karlsruhe, Germany, 1990.
[23] H.J. Blaß, M. Frese, P. Glos, J. Denzler, P. Linsenmann, A. Ranta-Maunus, Zuverlässigkeit von Fichten-Brettschichtholz mit modifiziertem Aufbau, Technical Report, Universitätsverlag Karlsruhe, Karlsruher Institut für Technologie (KIT), Karlsruhe, Germany, 2009, https://doi.org/10.5445/KSP/1000008462.
[24] M. Frese, H.J. Blaß, Numerical description of size and load configuration effects in glulam structures, in: of Statistics and Probability in Civil Engineering (ICASP12), The University of British Columbia, Vancouver, Canada, 2015, https://doi.org/10.14288/1.0076135.
[25] M. Frese, Computergestützte Verfahren zur pragmatischen Beurteilung der Tragwiderstände von Brettschichtholz: Zusammenfassung exemplarischer Simulationsstudien, Habilitation, KIT Scientific Publishing, Karlsruhe, Germany, 2016, https://doi.org/10.5445/KSP/1000052710.
[26] M. Frese, H.J. Blaß, Reliability of large glulam members Part 1: Data for the assessment of partial safety factors for the bending strength, in: Proceedings of the International Network on Timber Engineering Research (INTER) Meeting 49, Paper INTER/49-17-1, Graz, Austria, 2016.
[27] M. Frese, An analytical validation of numerically determined load configuration factors, in: Proceedings of the 2016 World Conference on Timber Engineering (WCTE 2016), Vienna, Austria, 2016.
[28] M. Frese, C. Sandhaas, On the question whether the volume of glulam bending members changes their reliability, in: Book of Abstracts: CompWood 2019, Växjö, Sweden, 2019, p. 76.
[29] G. Fink , A. Frangi , J. Kohler , Modelling the bending strength of glued laminated timber: Considering the natural growth characteristics of timber, *Proceedings of the International Council for Research and Innovation in Building and Construction: Working Commision W18 (CIB-W18) Meeting 46, Paper CIB-W18/46-12-1* , Vancouver, Canada , 2013 , pp. 211 – 225
[30] G. Fink, Influence of varying material properties on the load-bearing capacity of glued laminated timber, Ph.D. thesis, ETH Zurich, Zurich, Switzerland, 2014, https://doi.org/10.3929/ethz-a-010294974.
[31] G. Fink, A. Frangi, J. Kohler, Bending tests on GLT beams having well-known local material properties, Mater. Struct. 48 (2015) 3571–3584, https://doi.org/10.1617/s11527-014-0424-2.
[32] G. Fink, A. Frangi, J. Kohler, Probabilistic approach for modelling the load-bearing capacity of glued laminated timber, Eng. Struct. 100 (2015) 751–762, https://doi.org/10.1016/j.engstruct.2015.06.015.
[33] C. Tapia Camú, S. Aicher, A stochastic finite element model for glulam beams of hardwoods, in: Proceedings of the 2018 World Conference on Timber Engineering (WCTE 2018), Seoul, Republic of Korea, 2018.
[34] C. Tapia Camú, S. Aicher, Applying the XFEM method to the simulation of tensile failure in timber boards and finger-joints in a glulam strength model, in: Book of Abstracts: CompWood 2019, Växjö, Sweden, 2019. p. 110.
[35] C. Tapia Camú, Variation of mechanical properties in oak boards and its effect on glued laminated timber: Application to a stochastic finite element glulam strength model, Ph.D. thesis, Universität Stuttgart, Stuttgart, Germany, 2022, https://doi.org/10.18419/opus-12111.
[36] G. Kandler, M. Lukacevic, C. Zechmeister, S. Wolff, J. Füssl, Stochastic engineering framework for timber structural elements and its application to glued laminated timber beams, Constr. Build. Mater. 190 (2018) 573–592, https://doi.org/10.1016/j.conbuildmat.2018.09.129.
[37] R.H. Falk, F. Colling, Laminating effects in glued-laminated timber beams, Journal of Structural Engineering 121 (1995) 1857–1863, https://doi.org/10.1061/(ASCE)0733-9445(1995)121:12(1857).
[38] C. Vida, M. Lukacevic, J. Eberhardsteiner, J. Füssl, Modeling approach to estimate the bending strength and failure mechanisms of glued laminated timber beams, Eng. Struct. 255 (2022) 113862, https://doi.org/10.1016/j.engstruct.2022.113862.
[39] K. Hofstetter, C. Hellmich, J. Eberhardsteiner, Micromechanical modeling of solid-type and plate-type deformation patterns within softwood materials, A review and an improved approach, Holzforschung 61 (2007) 343–351, https://doi.org/10.1515/HF.2007.058.
[40] G. Kandler, M. Lukacevic, J. Füssl, An algorithm for the geometric reconstruction of knots within timber boards based on fibre angle measurements, Constr. Build. Mater. 124 (2016) 945–960, https://doi.org/10.1016/j.conbuildmat.2016.08.001.
[41] C. Hackspiel, K. de Borst, M. Lukacevic, A numerical simulation tool for wood grading model development, Wood Sci. Technol. 48 (2014) 633–649, https://doi.org/10.1007/s00226-014-0629-0.
[42] M. Lukacevic, J. Füssl, Numerical simulation tool for wooden boards with a physically based approach to identify structural failure, European Journal of Wood and Wood Products 72 (2014) 497–508, https://doi.org/10.1007/s00107-014-0803-y.
[43] M. Lukacevic, J. Füssl, J. Eberhardsteiner, Discussion of common and new indicating properties for the strength grading of wooden boards, Wood Sci. Technol. 49 (2015) 551–576, https://doi.org/10.1007/s00226-015-0712-1.
[44] Abaqus, Abaqus 2021 HF5, Dassault Systèmes Simulia Corp., Providence, RI, USA, 2021.
[45] M. Lukacevic, J. Füssl, R. Lampert, Failure mechanisms of clear wood identified at wood cell level by an approach based on the extended finite element method, Eng. Fract. Mech. 144 (2015) 158–175, https://doi.org/10.1016/j.engfracmech.2015.06.066.
[46] M. Lukacevic, W. Lederer, J. Füssl, A microstructure-based multisurface failure criterion for the description of brittle and ductile failure mechanisms of clear-wood, Eng. Fract. Mech. 176 (2017) 83–99, https://doi.org/10.1016/j.engfracmech.2017.02.020.
[47] S. Pech, M. Lukacevic, J. Füssl, A robust multisurface return-mapping algorithm and its implementation in Abaqus, Finite Elem. Anal. Des. 190 (2021) 103531, https://doi.org/10.1016/j.finel.2021.103531.
[48] F. Colling, Einfluß des Volumens und der Spannungsverteilung auf die Festigkeit eines Rechteckträgers: Herleitung einer allgemeinen Beziehung mit Hilfe der 2-parametrigen Weibull-Verteilung, Holz als Roh- und Werkstoff 44 (1986) 121–125, https://doi.org/10.1007/BF02612013.
[49] S. Pech, M. Lukacevic, J. Füssl, A hybrid multi-phase field model to describe cohesive failure in orthotropic materials, assessed by modeling failure mechanisms in wood, Eng. Fract. Mech. 271 (2022) 108591, https://doi.org/10.1016/j.engfracmech.2022.108591.
[50] S. Pech, M. Lukacevic, J. Füssl, Validation of a hybrid multi-phase field model for fracture of wood, Eng. Fract. Mech. 275 (2022) 108819, https://doi.org/10.1016/j.engfracmech.2022.108819.
[51] A. Hazen, Storage to be provided in impounding municipal water supply, Trans. Am. Soc. Civil Eng. 77 (1914) 1539–1640, https://doi.org/10.1061/taceat.0002563.